

# Prefrontal cortical distribution of muscarinic M2 and cannabinoid-1 (CB1) receptors in adult male mice with or without chronic adolescent exposure to $\Delta$ 9-tetrahydrocannabinol

Miguel Garzón <sup>1,2,\*</sup>, June Chan<sup>2</sup>, Ken Mackie<sup>3</sup>, Virginia M. Pickel<sup>2</sup>

<sup>1</sup>Departamento de Anatomía, Histología y Neurociencia, Facultad de Medicina UAM, 28029 Madrid, Spain,

<sup>2</sup>Feil Family Brain and Mind Research Institute, Weill Cornell Medicine, 407 East 61st Street, New York, NY 10065, USA,

<sup>3</sup>Linda and Jack Gill Center for Biomolecular Science, Department of Psychological and Brain Sciences, Indiana University, Bloomington, IN 47405, USA

\*Corresponding author: Department of Anatomy, Histology and Neuroscience, Medical School, Autónoma University of Madrid, Arzobispo Morcillo 4, 28029 Madrid, Spain. Email: miguel.garzon@uam.es

Chronic adolescent administration of marijuana's major psychoactive compound,  $\Delta$ 9-tetrahydrocannabinol ( $\Delta$ 9-THC), produces adaptive changes in adult social and cognitive functions sustained by prelimbic prefrontal cortex (PL-PFC). Memory and learning processes in PL-PFC neurons can be regulated through cholinergic muscarinic-2 receptors (M2R) and modulated by activation of cannabinoid-1 receptors (CB1Rs) targeted by  $\Delta$ 9-THC. Thus, chronic exposure to  $\Delta$ 9-THC during adolescence may alter the expression and/or distribution of M2Rs in PL-PFC neurons receiving CB1R terminals. We tested this hypothesis by using electron microscopic dual CB1R and M2R immunolabeling in adult C57BL/6 J male mice that had received vehicle or escalating dose of  $\Delta$ 9-THC through adolescence. In vehicle controls, CB1R immunolabeling was mainly localized to axonal profiles virtually devoid of M2R but often apposing M2R-immunoreactive dendrites and dendritic spines. The dendrites received inputs from CB1R-labeled or unlabeled terminals, whereas spines received asymmetric synapses exclusively from axon terminals lacking CB1Rs. Adolescent  $\Delta$ 9-THC significantly increased plasmalemmal M2R-immunogold density exclusively in large dendrites receiving input from CB1R-labeled terminals. In contrast, cytoplasmic M2R-immunogold density decreased in small spines of the  $\Delta$ 9-THC-treated adult mice. We conclude that  $\Delta$ 9-THC engagement of CB1Rs during adolescence increases M2R plasmalemmal accumulation in large proximal dendrites and decreases M2R cytoplasmic expression in small spines of PL-PFC.

**Key words:** cannabinoid; cholinergic; marijuana; prelimbic; ultrastructure.

## Introduction

There is increasing evidence that cannabis exposure in adolescence is a potential contributing factor to cognitive impairment and psychiatric vulnerability during adulthood (Rubino and Parolaro 2016). Cannabinoid consumption during ongoing brain maturation might interfere in neurodevelopmental processes essential for later optimal performance (Gruber and Pope Jr. 2002; Rubino et al. 2015; Bara et al. 2021). Delta-9-tetrahydrocannabinol ( $\Delta$ 9-THC) is the primary psychoactive component of marijuana and binds type-1 cannabinoid receptors (CB1R) whose mRNA and protein have a laminar distribution in the prefrontal cortex (PFC) (Matsuda et al. 1993; Ong and Mackie 1999; Egertová and Elphick 2000; Bodor et al. 2005). Activity-dependent retrograde CB1R activation reduces adenylyl cyclase and  $\text{Ca}^{2+}$  currents presynaptically, inhibiting neurotransmitter release (Castillo et al. 2012).

Cannabinoid exposure results in alterations in PFC activity and impairment of several PFC-based cognitive behaviors such as attention, working memory, or reversal learning (Egerton et al. 2006; Chen and Mackie 2020). Those deficits seem to be highly dependent on cannabinoid-modulated changes in cholinergic activity, and especially muscarinic actions in the prelimbic (PL)-PFC (Heidbreder and Groenewegen 2003). Moreover, cholinergic inhibition and decreased acetylcholine are significantly involved in the spatial memory impairment produced by  $\Delta$ 9-THC (Gessa et al. 1998; Mishima et al. 2002). Genetic deletion of CB1R also aggravates Alzheimer-like symptoms in murine models (Aso et al. 2018).

Gi-/Go-coupled muscarinic-2 receptors (M2R) are expressed in many glutamatergic pyramidal cells and in subpopulations of interneurons in the cerebral cortex (Hájos et al. 1998; Mrzljak et al. 1998). The M2Rs

are also highly expressed in afferent axon terminals, where they mediate the inhibition of the release of acetylcholine, glutamate, and other neurotransmitters (Mrzljak et al. 1993). This inhibition is independent of endocannabinoid signaling but may be significantly affected by the CB1R-mediated actions of  $\Delta$ 9-THC on both cholinergic and glutamatergic neurons, particularly those giving rise to the M2R-regulated hippocampal/PFC pathway (Kathmann et al. 2001; Wang and Yuan 2009). A critical involvement of CB1Rs in the displacement of plasticity-regulating transmitter systems and behavioral abnormalities resulting from chronic administration of  $\Delta$ 9-THC is suggested by the defects in synaptic plasticity and behaviors seen in CB1R  $-/-$  mice (Steiner et al. 1999; Kishimoto and Kano 2006). However, there are many existing gaps in our knowledge of the cellular sites and mechanisms by which complex executive functions in adulthood can be provoked by molecular changes that are initially primed by early use of marijuana. In this study, we used high-resolution electron microscopic immunolabeling to fill these gaps, specifically in the PFC where the late developing neural circuitry is potentially more sensitive to cannabinoid-regulated synaptic plasticity affecting both cognitive and reward functions (Rubino and Parolaro 2008; Bara et al. 2021; Garzón et al. 2021). Thus, in the present study, we determined the subcellular relationships between CB1R and M2R activation sites in naïve male mice. In addition, we sought to assess whether chronic administration of an escalating dose of  $\Delta$ 9-THC during adolescence alters the expression and/or distribution of M2R in neuronal compartments targeted by CB1R-containing axon terminals in the PL-PFC of adult male C57Bl6J mice. The results show selective targeting of large M2R-expressing dendrites by CB1R axon terminals, as well as a previously unrecognized effect of repeated adolescent administration of  $\Delta$ 9-THC on M2R distribution in dendritic profiles segregated with respect to their size and input from CB1R-containing axon terminals. The findings have important implications for understanding potential therapeutic targets to treat the effects of adolescent cannabis use.

## Materials and methods

### Animals and drug treatment

All experimental procedures were carried out in accordance with the National Institutes of Health Guidelines for the Care and Use of Laboratory Animals and were approved by the Institutional Animal Care and Use Committees (IACUC) at Weill Cornell Medicine. All efforts were made to minimize animal suffering and to use the minimally necessary number of animals. C57BL/6 J male mice were obtained commercially from Jackson Laboratory (Bar Harbor, ME) immediately after weaning at postnatal day (PD) 21 and reared in groups of 4–5 mice/cage from weaning to adulthood at PD 70 (Spear 2000). C57BL/6 J mice are chosen because they are

readily available and well characterized with respect to the behavioral effects of  $\Delta$ 9-THC (Laaris et al. 2010; Wise et al. 2011). The animals were kept in a temperature- and humidity-controlled environment and maintained with HEPA-filtered air on a 12-h light/dark cycle (lights on from 7 AM to 7 PM). Food and water were available ad libitum.

Nitrogen gas was used to evaporate the ethanol from a solution containing  $\Delta$ 9-THC (100 mg/mL), which was provided by the Drug Supply Program of the National Institute on Drug Abuse (Bethesda, MD, USA). The  $\Delta$ 9-THC residue was dissolved using a modification of that described by Burston et al. (2010), in which the residue is briefly heated at  $<100$  °C in 0.9% NaCl (saline) solutions containing 4%, 8%, or 14% Tween 80, used respectively to prepare 2.5, 5.0, and 10 mg/kg doses of  $\Delta$ 9-THC. Each of these doses was administered to male mice by once daily intraperitoneal injections on five consecutive days totaling 15 days from postnatal day (PD) 28 to 43. This age range corresponds to the adolescent transition from younger to older neurobehavioral characteristics in rodents (Spear 2000). This paradigm was chosen from previous studies indicating its similarity to escalating cannabis use in teenagers (Lopez-Rodriguez et al. 2014). The mice were assigned randomly to either the experimental group receiving  $\Delta$ 9-THC or the control group receiving equal quantities of the vehicle (saline and Tween 80). After completion of the last injection on PD 43, the mice were returned to their home cages where they remained without further injections until adulthood at PD 70. The prefrontal cortical tissue from mice in each treatment group was analyzed by electron microscopic dual immunolabeling by individuals unaware of whether the mice received vehicle or  $\Delta$ 9-THC. The brain tissues from adult mice receiving either vehicle or  $\Delta$ 9-THC during adolescence were processed for dual electron microscopic immunolabeling of the CB1R and muscarinic M2R, to determine (i) relevant sites for M2R activation and interactions involving CB1R and (ii) whether repeated adolescent administration of  $\Delta$ 9-THC alters the adulthood subcellular distribution of M2R and/or its ultrastructural relationships with CB1R-containing profiles.

### Antisera

The M2R immunoreactivity was detected with a rabbit polyclonal antiserum (product number AMR-002, Lot AN-08, Alomone Labs Ltd, Jerusalem, Israel) directed against a synthetic fusion protein containing glutathione S-transferase fused to a part of the i3 intracellular loop of human M2R (residues 225–356) (Bonner et al. 1987; Peralta et al. 1987; Levey et al. 1991). The identity of the fusion protein was confirmed by DNA sequencing and SDS-PAGE western blotting of rat brain membranes. The specificity of the M2R antiserum has been previously verified by loss of immunoreactivity in brain tissue processed using preadsorbed antisera in wild-type mice, or unadsorbed M2R antisera in M2R knockout mice (Garzón and Pickel 2006, 2016). In the present study, we

also confirmed the absence of labeling for M2R in the mouse mPFC in negative control experiments after prior incubation in buffer solution without M2R antiserum (data not shown). The pattern of labeling seen using the M2R antiserum in the present study was similar to that previously observed in the mPFC (Levey et al. 1991; Hohmann et al. 1995) and known M2R mRNA localization (Weiner et al. 1990; Vilaró et al. 1992, 1994).

The CB1R was identified using an affinity-purified polyclonal antibody raised in guinea pig against the full C terminus of the rat CB1R [residues 401–473] (Wager-Miller et al. 2002; Berghuis et al. 2007) peptide sequences within the C-terminus. The guinea pig CB1R antibody used herein shows no immunoreactivity in CB1R<sup>-/-</sup> cortex (Fitzgerald et al. 2012). Moreover, CB1R immunoreactivity pattern in the present study is in accordance with cortical CB1R labeling observed using the same (Fitzgerald et al. 2012, 2013) or other CB1R antibodies raised in rabbit (Katona et al. 1999, 2001; Bodor et al. 2005), and it is also consistent with previously reported CB1R mRNA and ligand binding sites (Herkenham, Lynn, De Costa, et al. 1991; Herkenham, Lynn, Johnson, et al. 1991; Marsicano and Lutz 1999; Bedse et al. 2014).

### Tissue preparation

Preparation of the tissue prior to immunocytochemistry was done according to procedures described by Milner et al. 2011. Groups of 5 vehicle- and 5 THC-injected male C57BL/6 J mice weighing 20–25 g were deeply anesthetized by intraperitoneal injection of 150 mg/kg sodium pentobarbital. The brains were fixed by vascular perfusion through the left ventricle of the heart with (i) 5 mL of heparin (1,000 U/mL) in saline, (ii) 30 mL of 3.75% acrolein (Polysciences, Warrington, PA) in a solution of 2% paraformaldehyde in 0.1 M phosphate buffer (PB), and (iii) 150 mL of 2% paraformaldehyde in 0.1 M PB. The brains were removed from the cranium, dissected, and postfixed by immersion for 30 min in 2% paraformaldehyde in 0.1 M PB. Brains were then transferred to 0.1 M PB at 4°C and coronal sections at 40- $\mu$ m thickness were cut through the frontal region including the prelimbic sector of mPFC (PL-PFC) at 1.94 mm anterior to Bregma (Paxinos and Franklin 2001) on a Leica Vibratome VT1000 S (Leica Microsystems, Bannockburn, IL, USA). These sections of tissue were incubated for 30 min in a solution of 1% sodium borohydride in 0.1 M PB to remove excess of active aldehydes and rinsed in 0.1 M PB until bubbles disappeared. After extensive rinsing in 0.1 M Tris-buffered saline (TS), the sections were blocked for 30 min in 0.5% bovine serum albumin (BSA) in 0.1 M TS to minimize nonspecific staining and then processed for dual-immunocytochemical labeling.

### Dual immunocytochemical labeling

Free-floating sections prepared as described above were processed for dual immunoperoxidase and immunogold–silver detection of CB1R and M2R, respectively, using a

protocol previously described by Chan et al. (1990). All the incubations were carried out at room temperature with continuous agitation on a rotator and were followed by several rinses in 0.1 M TS, 0.1 M PB, and 0.01 M phosphate-buffered saline (PBS). The primary antisera against CB1R and M2R were raised in guinea pigs and rabbits, respectively, and therefore could be recognized by appropriate species-specific secondary antibodies. Sections prepared as described above were incubated for 36–42 h at 4 °C in a solution containing: (i) guinea pig polyclonal antiserum for CB1R (diluted 1:3,200 for immunoperoxidase) and (ii) rabbit polyclonal antiserum for M2R (diluted 1:100 for immunogold). After incubation in these primary antisera, tissue sections were first processed for immunoperoxidase and afterwards for immunogold labeling.

For the immunoperoxidase visualization of antigens, the avidin–biotin peroxidase complex (ABC) method (Hsu et al. 1981) was used. For this, the incubation in primary antisera was followed by incubation in secondary biotinylated antibody (donkey anti-guinea pig IgG, 1:200, Jackson ImmunoResearch Laboratories Inc, West Grove, PA, USA) for 30 min and then in ABC (1:100, Vectastain Elite Kit, Vector Laboratories, Burlingame, CA, USA) for another 30 min. The immunoreactivity bound to the tissue was visualized by a 6-min incubation in 0.022% 3,3'-diaminobenzidine (DAB, Aldrich, Milwaukee, WI, USA) and 0.003% hydrogen peroxide in 0.1 M TS.

These sections were then prepared for silver-enhanced immunogold labeling. Thus, they were rinsed in 0.1 M TS, transferred to 0.01 M PBS for 1 h, blocked for 10 min in 0.8% BSA and 0.1% gelatin in 0.01 M PBS, and incubated for 2 h in colloidal gold (1.25 nm)-labeled antibody (goat anti-rabbit IgG, 1:25, Nanoprobes, Yaphank, NY, USA). After this, the sections were fixed for 10 min in 2% glutaraldehyde in 0.01 M PBS and washed in 0.2-M citrate buffer, pH 7.4, prior to silver enhancement using a silver solution IntenSE<sup>-</sup>M kit (Amersham, Arlington Heights, IL, USA) for 8 min.

### Electron microscopy

Immunolabeled sections for electron microscopy were postfixed in 2% osmium tetroxide in 0.1 M PB for 45 min, dehydrated through a graded series of ethanols (30°–50°–70°–95°–100°) and propylene oxide, and incubated overnight in a 1:1 mixture of propylene oxide and Epon (EMbed-812; Electron Microscopy Sciences, Fort Washington, PA). The sections were transferred to 100% Epon for 2 h prior to flat embedding in Epon between two sheets of Aclar plastic (Allied Signal, Pottsville, PA, USA).

The area containing the flat-embedded mPFC was mounted and glued on top of Epon blocks and trimmed into a deep layer PL-PFC trapezoid. Ultrathin sections (70 nm) were cut from the outer surface of this tissue with a diamond knife (Diatome, Fort Washington, PA) by using an ultramicrotome (Leica UC6; Leica Microsystems, Buffalo Grove, Illinois). The sections were collected on 400-mesh copper grids, counterstained with uranyl acetate and lead citrate (Reynolds 1963), and examined

with a Tecnai Biotwin 12 (Serial # D271) electron microscope (FEI Company, Hillsboro, OR). Only sections near the surface of the tissue at the Epon–tissue interface were examined to reduce false negatives due to inadequate penetration of antisera. The ultrathin sections were initially examined at low magnification (8,000 $\times$ ) to identify the surface of the tissue and ensure observation of those regions containing immunolabeling for both CB1R and M2R. These were then magnified to 18,500 $\times$  and captured as digital images with an interfaced digital camera (Advanced Microscopy Techniques Corporation, Danvers, MA, USA) for examination and profile counting without further selection of the fields.

### Data analysis

A total of 10 immunolabeled Vibratome sections (five each from naive or  $\Delta 9$ -THC-treated mice) from 10 different animals were studied. About 546 total images for quantification were collected from PL-PFC of  $\Delta 9$ -THC-treated and control vehicle-administered mice. A profile was selectively immunoperoxidase labeled when the electron dense precipitate made it appear considerably darker than morphologically similar profiles located in the neighboring neuropil. Immunogold-labeled structures were identified as those containing two or more gold particles or a single gold particle on the plasma membrane of small axonal or dendritic profiles (Garzón et al. 1999; Garzón and Pickel 2000). Thus, in those small profiles, even a single particle was considered positive immunogold-labeling, since virtually no gold–silver deposits were seen over myelin and other tissue elements not known to express muscarinic receptors. This approach was validated by the little if any spurious distribution of gold–silver deposits in the tissue or plastic embedding matrix.

The classification of identified cellular elements was based on the descriptions of Peters et al. 1991. Axon terminals were identified by the presence of numerous synaptic vesicles and were at least 0.2  $\mu\text{m}$  in diameter. Small unmyelinated axons were <0.2  $\mu\text{m}$  and rarely contained small vesicles. Neuronal somata were identified by the presence of a nucleus, Golgi apparatus, and rough endoplasmic reticulum. Dendrites usually contained abundant endoplasmic reticulum and were distinguished from unmyelinated axons by their larger diameter and/or abundance of uniformly distributed microtubules. In addition, dendrites were in many cases postsynaptic to axon terminals. Dendritic spines lacked the mitochondria and endoplasmic reticulum typical of dendrite shafts, were small in diameter (less than 0.5  $\mu\text{m}$ ), and often showed electron-dense postsynaptic specializations underneath axon terminal contacts. Asymmetric synapses were recognized by thick postsynaptic densities (asymmetric synapses, type Gray I), while symmetric synapses had thin pre- and postsynaptic specializations (symmetric synapses, type Gray II) (Gray 1959). Zones of closely spaced parallel plasma membranes, which lacked discernible synaptic

densities, but were otherwise not separated by glial processes, were defined as appositions or nonsynaptic contacts. Glial processes were identified by their irregular shape, which followed the contours of neuronal profiles. The glial cytoplasm also often contained bundles of filaments.

All CB1R and/or M2R-immunolabeled processes ( $n = 3,875$ ) were counted from an area of 15,496.5  $\mu\text{m}^2$ , with an area of at least 1,062.4  $\mu\text{m}^2$  examined in each animal and vibratome section. They were categorized as dendrites, spines, axon terminals, small unmyelinated axons, neuronal cell bodies, or glial processes. In addition, morphologically recognizable synaptic relationships of each labeled profile were also quantified, as well as nonsynaptic appositional contacts among M2R-immunoreactive and/or CB1R-labeled profiles. M2R-immunogold particles were further analyzed with respect to their subcellular localization in contact (plasmalemmal) or not (cytoplasmic) with the plasma membrane of individual profiles. Electron microscopic images were captured by an investigator blind to whether the tissue was derived from mice receiving vehicle or  $\Delta 9$ -THC.

Area density (number of CB1R or M2R single- and CB1R + M2R dual-immunolabeled profiles per analyzed cross-sectional surface) was assessed for each vibratome section. Besides the area density for total profiles, individual area densities were calculated for each cellular profile type. Analysis of Variance (ANOVA)s were used to evaluate whether there was significant variability in immunolabeling area density with respect to (i) different animals or (ii) different treatment. In addition, MCID Elite software version 7.0 (InterFocus Ltd, Cambridge, UK) was used to measure the cross-sectional diameter, major axis and minor axis length, cytoplasmic area, plasmalemmal perimeter and form factor of M2R-immunolabeled profiles. These latter measurements were used to calculate between-group comparisons (Student's t-test) in the following parameters in dendrites and spines: (i) average diameter; (ii) area, (iii) perimeter, (iv) cytoplasmic density of M2R immunogold; and (v) plasmalemmal density of M2R immunogold. ANOVAs were used to determine whether there was significant variability in immunolabeling regarding several factors such as treatment, targeting by CB1R-immunolabeled terminals or size. Contingency tests using chi-square were used for assessing interactions among those factors.

Since dendritic shafts are not a homogeneous structure regarding their inputs, M2R-immunolabeled dendrites were statistically separated by size into small, medium, and large categories using cluster analysis of their average diameter. Larger dendrites are expected to be proximal to the cell body and are more likely than small- and medium-sized dendrites to receive symmetric inhibitory-type synaptic contacts. The latter dendrites, on the contrary, are likely to be receptive mainly of asymmetric excitatory-type contacts. The small dendrites are prospectively the most distal to the soma, tending to have the highest input resistance and to receive inputs from

axons coming majorly from distant cortical or extracortical sources. JMP Statistical Discovery from SAS (Cary, NC, USA) was used to determine statistically significant ( $P < 0.05$ ) differences in M2R density in dendritic profiles of each size range in the PL-PFC of the mice receiving vehicle or  $\Delta 9$ -THC as adolescence. Two-way ANOVA JMP statistics was also used to compare M2R-labeled dendritic profiles of each of the three sizes with and without synaptic contacts from CB1R-labeled axon terminals.

The electron micrographs used for the figures were acquired with an AMT digital camera (Advanced-Microscopy Techniques Corporation, Danvers, MA) on a Microsmart Computer using a Windows 2000 operating system. To build and label the composite illustrations, Adobe Photoshop (version 7.0; Adobe Systems Inc., Mountain View, CA) was used for adjustment of brightness and contrast of the acquired digital images. From Photoshop, the images were then imported into Microsoft Office PowerPoint (Microsoft Corporation, Redmond, WA) to add lettering and assembling composite plate figures.

## Results

Both M2R and CB1R had quite similar laminar distributions in the PL-PFC. However, the M2R labeling was observed in both neuropil processes and cell membranes delineating clear neuronal somata, whereas CB1R immunoreactivity had a more punctate or varicose pattern suggestive of an axonal localization. Electron microscopy confirmed that in the mouse PL-PFC CB1R immunolabeling is mainly localized to small unmyelinated axons and axon terminals, almost none of which contained M2R but often apposed M2R-immunoreactive profiles. M2R immunolabeling was also localized to axons, but it was more often seen within the cytoplasm or on extrasynaptic plasma membranes of dendrites. M2R labeling was prevalent in (i) varying sizes of dendritic shafts that were contacted by CB1R-labeled or unlabeled terminals, and (ii) in dendritic spines receiving asymmetric synapses from axon terminals without detectable CB1R immunoreactivity. The following sections elaborate on the subcellular distribution of M2R and CB1R receptors detected by immunogold and immunoperoxidase labeling in the PL-PFC.

### Subcellular localization

Immunolabeling for M2R and CB1R was observed in similar types of profiles in the PL-PFC of adult male mice that received either  $\Delta 9$ -THC or vehicle injections during adolescence. However, the PL-PFC of the  $\Delta 9$ -THC and vehicle-injected mice significantly differed in the subcellular distribution of M2R in dendritic spines as well as in dendritic shafts distinguished by their size.

The utilization of immunogold as a marker enabled precise subcellular resolution for M2R identification. As compared with immunogold, the high sensitivity of the immunoperoxidase method allowed detection of CB1R immunoreactivity in many more small profiles and

particularly in small unmyelinated axons. However, the peroxidase localization of CB1R to precise organelles was obscured in most profiles due to the intense electron density of the diffuse peroxidase reaction product. The global distributions of CB1R or M2R labeling in different cellular compartments among animals were rather similar, and there were no apparent differences in frequencies or types of associations between differentially labeled profiles. Therefore, we pooled the data from different animals within each treatment group for the following descriptive analysis. Throughout the description of the results concerning localization of CB1R and/or M2R receptors, we will allude to numbers obtained exclusively from the vehicle-injected mice. Only in the last sections, explicitly addressing the effects of  $\Delta 9$ -THC administration in M2R-immunogold redistribution, the data obtained from the  $\Delta 9$ -THC-treated animals will be necessarily included.

### M2R distribution in different size dendrites

From 1,104 total M2R-immunoreactive profiles in the vehicle-treated group, 57.4% ( $n = 634$ ) (Table 1a) were M2R-immunogold labeled dendrites of different sizes, most often ranging from 0.5–3.7  $\mu\text{m}$  in diameter. Cluster analysis of dendritic average diameter classified M2R-immunolabeled dendrites as belonging to small ( $\leq 0.6 \mu\text{m}$ ), medium (0.6–0.8  $\mu\text{m}$ ), or large ( $> 0.8 \mu\text{m}$ ) categories. In these dendrites, M2R immunoreactivity was mainly distributed heterogeneously within the cytoplasm in larger dendrites (Figs 1b, c and 2a) and frequently localized to endomembranes resembling smooth endoplasmic reticulum (Fig. 2c and d), but M2R was also seen on portions of plasma membrane adjacent to incoming afferents especially in smaller dendrites (Figs 1a, 2b and c).

Most of the dendritic plasmalemmal particles were seen on portions of the plasmalemma not receiving synaptic input from axon terminals but apposing unmyelinated axons or close to asymmetric excitatory-type synapses (Figs 1a, 2c, and 3). In rare cases, M2R immunogold was in contact with the postsynaptic membrane specialization of asymmetric synapses or plasmalemmal segments apposing other M2R-labeled dendrites (Fig. 1d).

The M2R-immunoreactive dendrites received both asymmetric ( $n = 75$ ; 70.8%) and symmetric ( $n = 31$ ; 29.2%) synapses (Figs 1 and 2). Terminals containing M2R comprised only 21.7% ( $n = 23$ ) of the total inputs to M2R-immunolabeled dendrites. The remaining inputs were from CB1R-labeled ( $n = 55$ ; 51.9%) (Fig. 1b–d) or unlabeled axon terminals ( $n = 28$ ; 26.4%) (Figs 1c and 2c).

### CB1R distribution in axon terminals contacting M2R-immunolabeled dendritic and somatic profiles

Axon terminals accounted for about half the total CB1R-labeled profiles in the PL-PFC ( $n = 289$ ; 54.3%)

**Table 1.** Distribution of CB1R- and/or M2R-immunolabeled cellular profiles in the PL-PFC of mice that received either vehicle or  $\Delta^9$ -THC. Records for a) single M2R or b) single CB1R and dual CB1R + M2R labelings are given as raw numbers (N) and as percentage (%) out from the total immunolabeled profiles for each category (single M2R, dual CB1R + M2R, single CB1R) in both treatment groups (vehicle,  $\Delta^9$ -THC). Data were collected from 10 Vibratome sections in 10 mice processed for dual labeling.

LABELING (a)			Single M2R labeling						
PROFILE			Terminals	Dendrites	Spines	Soma	Axons	Glia	Total
GROUP	Vehicle	N	215	634	89	8	110	29	1085
		%	19.30	63.11	4.40	0.72	9.87	2.60	100
	$\Delta^9$ -THC	N	324	925	116	12	120	38	1535
		%	19.97	65.11	4.44	0.74	7.40	2.34	100
LABELING (b)			Single CB1R labeling			Dual CB1R + M2R labeling			
PROFILE			Terminals	Axons	Total	Terminals	Axons	Total	
GROUP	Vehicle	N	274	239	513	15	4	19	
		%	53.41	46.59	100	78.95	21.05	100	
	$\Delta^9$ -THC	N	373	334	707	14	2	16	
		%	52.76	47.24	100	87.50	12.50	100	

(Table 1B). Both in terminals and in small axons, CB1R-immunoperoxidase reaction product usually filled the whole profile and prevented visualization of CB1R associated to specific organelles (Figs 1, 2b, 3, and 4). Most CB1R-immunolabeled axon terminals were devoid of M2R immunoreactivity (Figs 1 and 5c), but a few of them contained also M2R ( $n=15/289$ ; 5.2%; Fig. 5d; Table 1b). CB1R-immunoperoxidase reaction product often obscured synaptic specialization, but occasionally the CB1R-immunolabeled terminals made recognizable synapses, apparently symmetric in most cases, with unlabeled ( $n=16$ ; Fig. 1c) and M2R-immunogold labeled ( $n=55$ ; Figs 1c–e, 3a and b, and 5d) dendrites. Other CB1R terminals were apposed without clearly defined specializations in the plane of section (Fig. 1c and d). As many as 171 contacts between CB1R-labeled terminals and M2R-immunogold dendrites were seen in our sample. In the larger dendrites contacted by CB1R-immunolabeled terminals, it was common to observe convergent input from other unlabeled or CB1R-labeled terminals (Fig. 1c). In some cases, a single CB1R-immunoreactive terminal contacted several M2R-immunoreactive dendrites (Fig. 1d).

The mean size of the M2R dendrites contacted by the CB1R-immunolabeled terminals was larger than that of M2R dendrites contacted only by unlabeled axon terminals. This is shown by significant differences in all dendritic size parameters analyzed (area,  $0.89 \pm 0.02 \mu\text{m}^2$  vs.  $1.15 \pm 0.03 \mu\text{m}^2$ ,  $F_{1,1557} = 43.44$ ;  $P < 0.0001$ ; perimeter,  $4.17 \pm 0.06 \mu\text{m}$  vs.  $4.98 \pm 0.10 \mu\text{m}$ ,  $F_{1,1557} = 47.79$ ;  $P < 0.0001$ ; average diameter,  $0.54 \pm 0.01 \mu\text{m}$  vs.  $0.59 \pm 0.01 \mu\text{m}$ ,  $F_{1,1557} = 12.21$ ;  $P < 0.0005$ ). Thus, CB-1-terminals contact cross-sectionally larger M2R-immunolabeled dendrites, presumably closer to the soma, than those terminals that do not contain CB1R. Moreover, M2R-immunogold density in M2R dendrites contacted by CB1R terminals is lower than in those contacted only by unlabeled terminals (total particles/area  $3.07 \pm 0.07/\mu\text{m}^2$

vs.  $2.45 \pm 0.12/\mu\text{m}^2$ ,  $F_{1,1557} = 19.14$ ;  $P < 0.0001$ ; cytoplasmic particles/area  $1.98 \pm 0.06/\mu\text{m}^2$  vs.  $1.69 \pm 0.09/\mu\text{m}^2$ ,  $F_{1,1557} = 6.69$ ;  $P < 0.0098$ ; plasmalemmal particles/perimeter\*10:  $1.45 \pm 0.06/\mu\text{m}$  vs.  $1.14 \pm 0.10/\mu\text{m}$ ,  $F_{1,1557} = 6.95$ ;  $P < 0.0085$ ).

CB1R-immunoreactive terminals were also frequently apposed with or without symmetric synapses onto neuronal somata ( $n=8$ ). These terminals frequently expanded in large appositional contacts with a single soma that had several contacts from apparently different CB1R-immunoreactive terminals in cross-section.

The majority of these somata showed morphological features characteristic of aspiny interneurons (Peters et al. 1991). The M2R immunogold in somata was mainly associated with tubulovesicular membranes resembling endoplasmic reticulum (Fig. 1a).

### CB1R distribution in small unmyelinated axons apposing M2R-immunolabeled profiles

CB1R-immunolabeled small unmyelinated axons (<0.2 mm in cross-section) were almost as prevalent as CB1R-labeled terminals ( $n=243/532$ ; 45.7%; Table 1b) among PL-PFC CB1R-labeled profiles (Figs 2a and b, and 5a, b, and e). They were usually distributed randomly through the neuropil and were often seen within a bundle of other labeled and unlabeled axons (Fig. 5a and b). CB1R distribution in small axons appeared homogeneous in most profiles (Fig. 2), but in some favorable longitudinally sectioned axons, CB1R immunoreactivity could be identified along distinct segments of the same axon (Fig. 5b). CB1R-labeled small axons often apposed M2R-immunoreactive profiles, especially small unmyelinated axons expressing plasmalemmal M2R-immunogold (Fig. 5a and b) or M2R-immunoreactive terminals (Fig. 5e). Dually immunolabeled axons for CB1R and M2R were uncommon (1.6%; 4/243) among CB1R-labeled small unmyelinated axons (Table 1b).

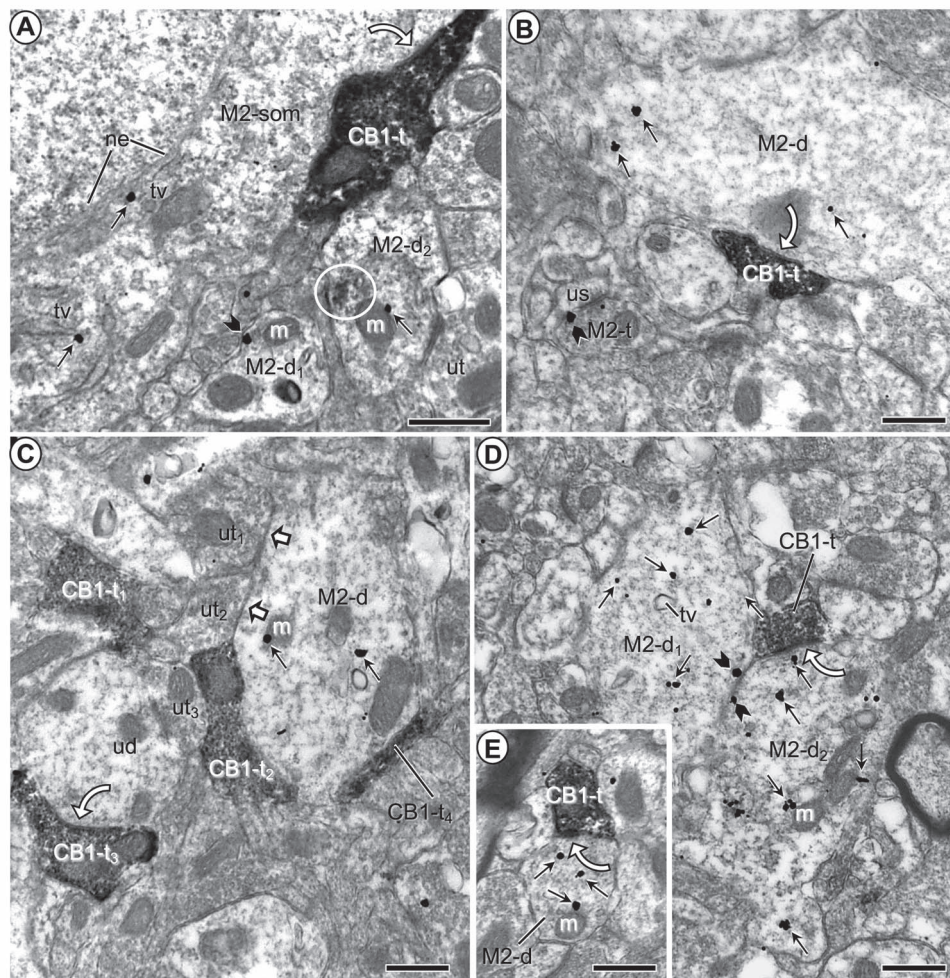


**Fig. 1.** Microscopic images showing M2R-immunogold distribution in somatodendritic profiles contacted by CB1R-labeled axon terminals in the PL-PFC of vehicle-injected mice. a) M2R immunogold particles are localized to the cytoplasm along the outer nuclear envelope (ne) and nearby tubulovesicles (tv) in a neuronal soma contacted by an axon terminal containing CB1R-immunoperoxidase reaction product. M2R immunogold particles are also seen in nearby dendrites (M2-d<sub>1,2</sub>), one of which shows partially aggregated (circle) restricted immunoperoxidase reaction product possibly reflecting infrequently observed DAB precipitate. b) M2R-immunogold particles are distributed within the cytoplasm of a large dendrite at a distance from a CB1R-peroxidase labeled axon terminal and are also present on the presynaptic plasma membrane of an axon terminal (M2-t) forming an asymmetric synapse with an unlabeled dendritic spine (us). c) M2R immunogold has a cytoplasmic distribution in a large dendrite apposed by axon terminals that are unlabeled (white block arrows) or contain CB1R-immunoperoxidase reaction product but lack clearly defined synaptic membranes. d) Two transversely sectioned large dendrites showing cytoplasmic and plasmalemmal M2R-immunogold particles have apposed plasma membranes and contacts from a single axon terminal containing dense CB1R-immunoperoxidase labeling. e) A small dendrite containing exclusively cytoplasmic M2R immunogold is contacted by a CB1R-immunoperoxidase labeled terminal. White curved arrows in (a–e) indicate putative symmetric synapses between CB1R-labeled axon terminals (CB1-t) and M2R-immunogold labeled soma (M2-som) and dendrites (M2-d; M2-d<sub>1</sub>; M2-d<sub>2</sub>). White block arrows in (c) show appositions between unlabeled terminals (ut) and the M2R-labeled dendrite. Small straight arrows in (a–e) and black block arrows in (a and b), respectively, identify cytoplasmic and plasmalemmal M2R-immunogold particles in somatodendritic profiles. CB1-t = immunoperoxidase labeling for CB1R in axon terminal. M = mitochondrion. Scale bars = 500 nm.

### M2R distribution in dendritic spines

M2R immunoreactivity was targeted to dendritic spines of the vehicle-treated group PL-PFC, although not as frequently as to dendritic shafts ( $n = 89$ ; 8.1% of M2R-labeled profiles) (Table 1a). In those spines, M2R-immunogold particles were usually localized to extrasynaptic portions of the plasma membrane. Although plasmalemmal M2R labeling was twice as frequent as cytoplasmic M2R labeling in dendritic spines, M2R immunogold also was regularly observed within spine cytoplasm (Fig. 4). M2R-labeled spines received asymmetric synapses from axon terminals that were mostly unlabeled (Fig. 4).

M2R-labeled spines only seldom received contacts from M2R-immunoreactive terminals (Figs 4e and 5c), but they were sometimes apposed to CB1R-immunolabeled small unmyelinated axons or axon terminals (Fig. 4a). However, in contrast with the results observed in dendritic shafts, M2R-immunogold density in spines was not related to targeting by axon terminals that were either CB1R immunoreactive or not (ANOVAs: total particles/area,  $F_{1,203} = 0.79$ ,  $P < 0.3734$ ; cytoplasmic particles/area,  $F_{1,203} = 0.26$ ,  $P < 0.6112$ ; plasmalemmal particles/perimeter\*10,  $F_{1,203} = 0.09$ ,  $P < 0.7682$ ). In fact, M2R-labeled spines received input almost exclusively

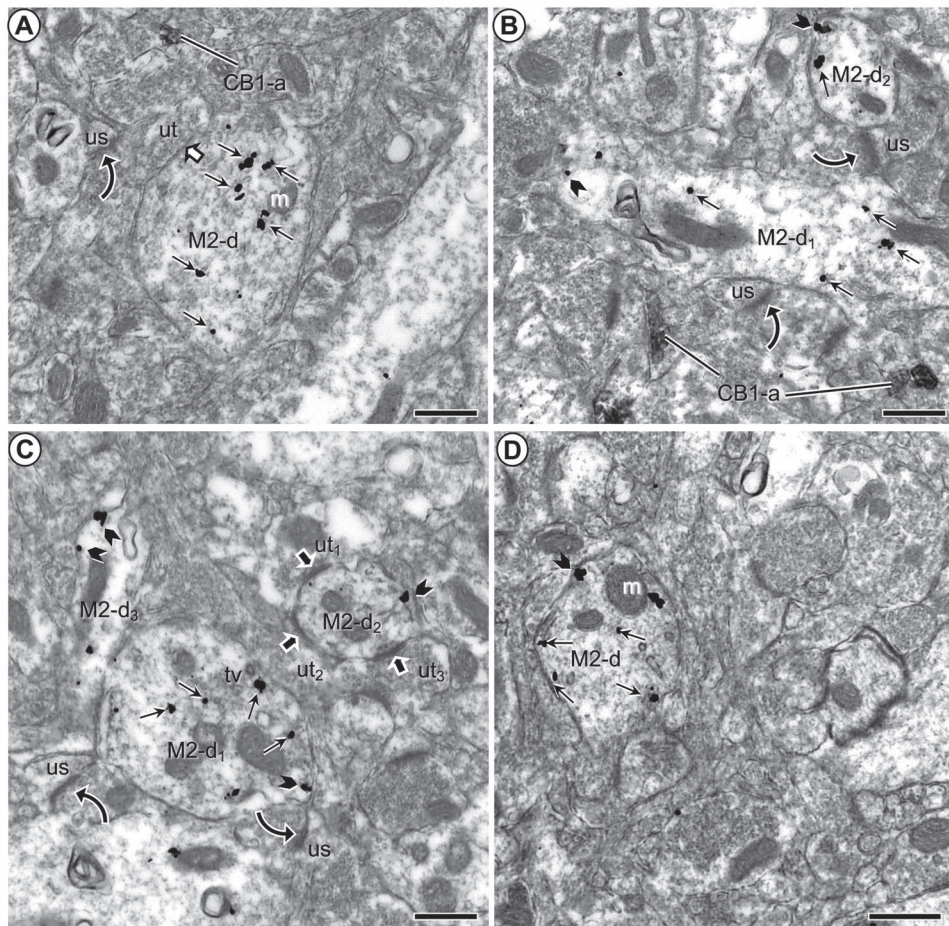


**Fig. 2.** M2R immunogold in dendrites without synaptic input from CB1R-immunoperoxidase labeled axon terminals in the PL-PFC of adult mice that received vehicle injections during adolescence. a) M2R immunogold is distributed in the cytoplasm of a large transversely sectioned dendrite without contact from axon terminals containing CB1R-immunoperoxidase product as seen in a more distant axon. The M2R-labeled dendrite receives synaptic input from an unlabeled terminal and apposes an axon terminal forming an asymmetric synapse with an unlabeled dendritic spine. b) Medium-sized dendrites (M2-d<sub>1,2</sub>) cut respectively in either longitudinal or transverse planes show many cytoplasmic and a few plasmalemmal M2R-immunogold particles. Both dendrites are apposed to unlabeled axon terminals forming excitatory-type axospinous synapse. c) M2-immunogold particles are distributed both in the cytoplasm and on the plasma membrane of a large dendrite (M2-d<sub>1</sub>), but only on the plasma membrane of nearby smaller dendrites (M2-d<sub>2,3</sub>). M2-d<sub>2</sub> is distinguished by receipt of asymmetric synapses from unlabeled axon terminals. d) Prominent distribution of M2R immunogold on endomembranes that are near the plasma membrane. Small straight arrows in (a–d) and black block arrows in (b–d), respectively, show cytoplasmic and plasmalemmal M2R-immunogold particles in varying size dendrites (M2-d). White block arrow in (a) indicates a symmetric synapse between unlabeled terminals (ut) and the M2R-labeled dendrite. Curved black arrows indicate asymmetric axospinous synapses. Black block arrows mark asymmetric synapses onto a dendrite containing M2R immunogold. CB1-a = CB1R-labeled axons in (a–c). m = mitochondrion; us = unlabeled spine; ut = unlabeled terminal. Scale bars = 500 nm.

from non-CB1R-containing terminals making asymmetric excitatory-type synapses. CB1R-immunoreactive terminals targeted mainly dendritic shafts and somata; contacts with spines were scarce and habitually located not on the spine head but in the neck of the spine.

### M2R distribution on plasmalemmal membranes of axon terminals targeting unlabeled dendrites and spines

M2R-immunogold particles were detected in many axonal profiles in the PL-PFC, comprising both axon terminals ( $n=240$ ) and small unmyelinated axons ( $n=114$ ) (Table 1a). The M2R-immunoreactive axon terminals were generally oval or round in shape, contained numerous small synaptic vesicles and one or more mitochondria, and were less than  $1.1 \mu\text{m}$  in average cross-sectional diameter. In most terminals,

M2R immunogold was seen on the plasma membrane (Figs 1b and 5c and e–g). M2R-immunogold particles were prevalent along extrasynaptic plasma membranes (Figs 1 and 5f) and more rarely localized to the presynaptic specialization (Fig. 5e and f). M2R-gold particles were more rarely seen in the terminal cytoplasm, in which case they were most commonly observed on the membranes of small synaptic vesicles (Fig. 5c and g) and/or near to the presynaptic membrane (Fig. 1b). M2R-immunoreactive axon terminals formed synapses and/or apposed dendrites and spines that were unlabeled (Figs 1b and 5c, e, and f) or also contained M2R immunolabeling (Fig. 4e). The synapses formed with M2R-labeled dendrites were asymmetric (78.3%;  $n=18$ ) or symmetric (21.7%;  $n=5$ ), whereas those established onto M2R-labeled spines were invariably asymmetric (Figs 4 and 5). In addition to the synaptic associations, 26 contacts with

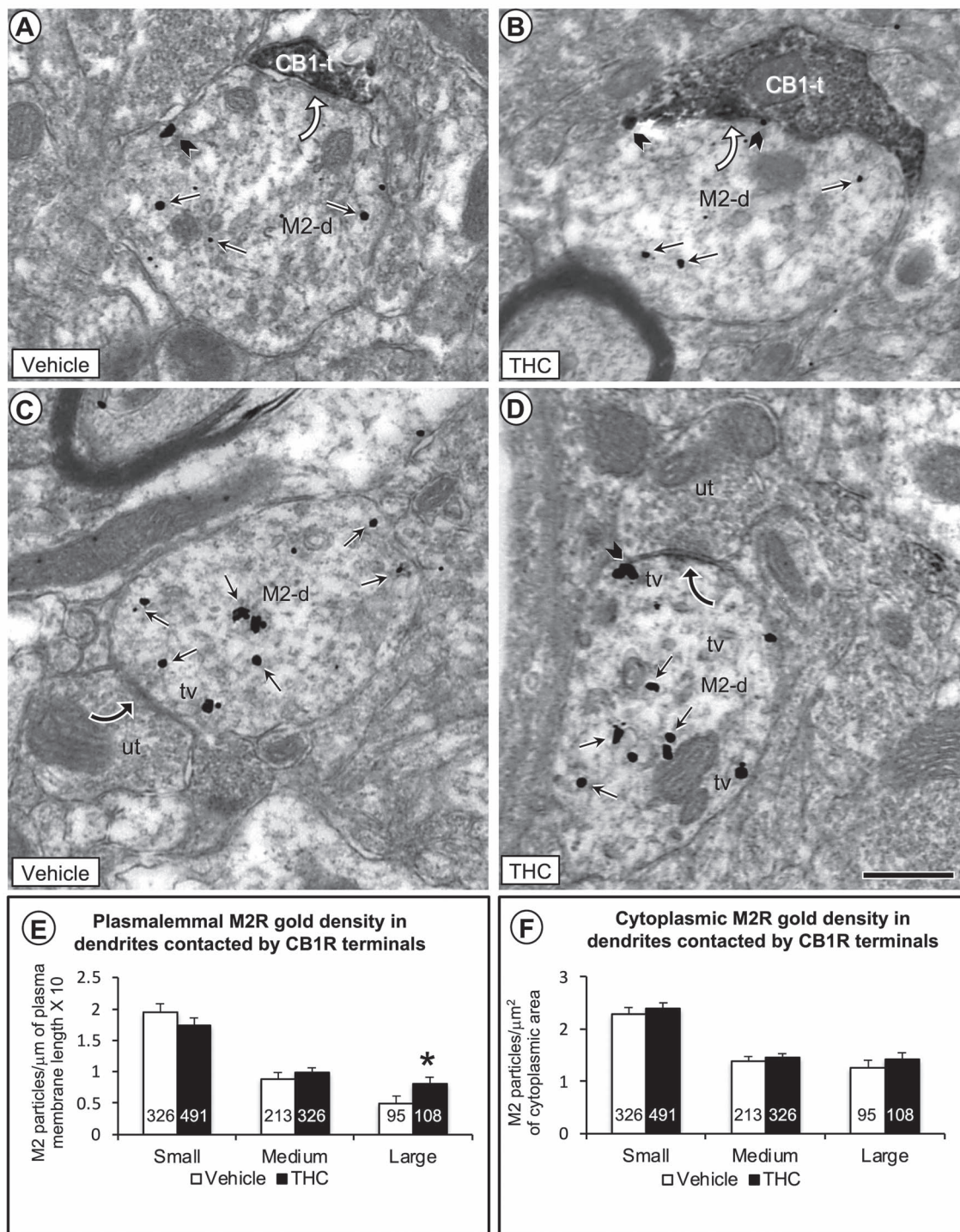


**Fig. 3.** Electron microscopic data comparing the density of M2R immunogold in plasmalemmal and cytoplasmic compartments of large dendritic shafts contacted by CB1R-labeled and unlabeled axon terminals in the PL-PFC of adult mice that received vehicle or THC during adolescence. In a–d), small straight arrows show cytoplasmic and black block arrows plasmalemmal M2R-immunogold particles in large dendrites (M2-d). a and b) As compared to vehicle, the THC-pretreated mice show a qualitative increase in number of M2R immunogold particles on the plasma membrane of large dendrites contacted (curved white arrows) by axon terminals containing CB1R-immunoperoxidase labeling. c and d) In both vehicle and THC-pretreated mice, many M2R-immunogold particles are localized to tubulovesicles (tv) just below the plasma membrane in large dendrites receiving symmetric synapses (curved black arrows) from unlabeled axon terminals. The subsurface vesicles and M2R-immunogold particles are most evident in mice receiving THC compared to vehicle. e) Bar graphs showing a significant increase in the plasmalemmal density of M2R immunogold particles exclusively on the plasma membrane of large dendritic profiles in THC compared with vehicle-injected mice. f) Bar graphs showing no significant differences between vehicle and THC-recipient mice in cytoplasmic density of M2R-immunogold particles in large dendrites. Numbers inside the bars in E–F depict absolute numbers of M2R-immunolabeled dendrites for each category. Asterisk =  $P < 0.05$  ANOVA. Scale bar = 500 nm.

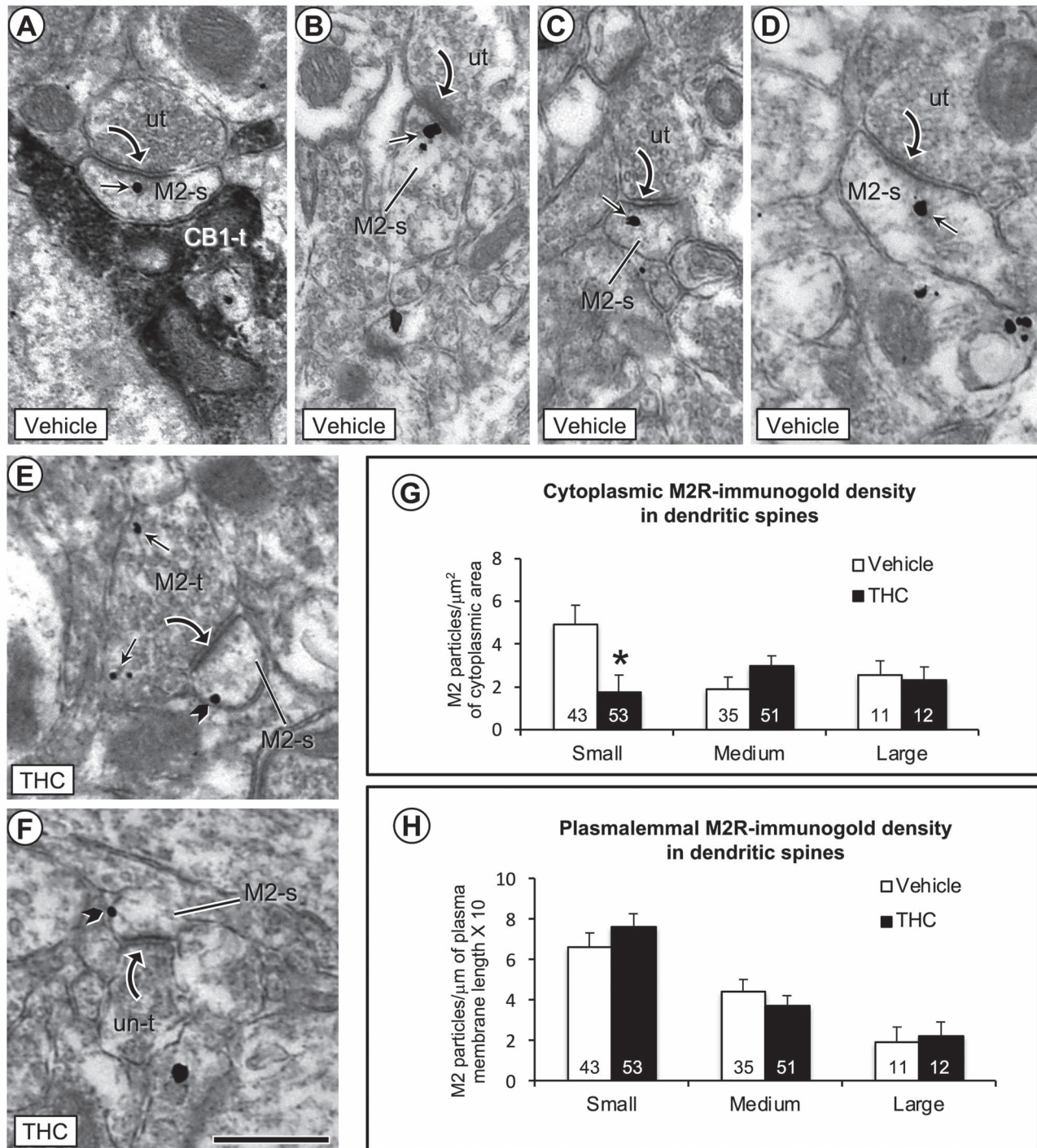


**Fig. 4.** Electron microscopic images (a–f) and bar graphs (g and h) showing a significant decrease in cytoplasmic and a nonsignificant increase in plasmalemmal density of M2R immunogold in small dendritic spines in the PL-PFC of THC compared with vehicle-injected mice. a) One M2R-immunogold particle is located within the cytoplasm of a small dendritic spine that receives an asymmetric synapse from an unlabeled axon terminal and an appositional contact from an axon terminal containing immunoperoxidase labeling for CB1R (CB1-t). b–d) In vehicle-injected mice, the M2R-immunogold particles in dendritic spines without contact from CB1R-labeled terminals are seen in the cytoplasm near or more distant to the postsynaptic membrane specialization at asymmetric synapses formed by unlabeled axon terminals. e and f) In THC-injected mice, M2R immunogold particles are less commonly seen in the cytoplasm and often located on lateral portions of the plasma membrane distant from asymmetric synapses in small dendritic spines. Small straight arrows and black block arrows respectively indicate cytoplasmic and plasmalemmal M2R-immunogold particles in varying sizes of dendritic spines (M2-s). Black curved arrow = asymmetric synapse from unlabeled terminals (ut) or M2R-labeled terminals to M2R-labeled dendritic spines. g and h) Bar graphs show a significant decrease in cytoplasmic and small, but nonsignificant increase in plasmalemmal M2R-immunogold particles in small dendritic spines of the THC compared to vehicle pretreated mice. Numbers inside the bars in G–H depict absolute numbers of M2R-immunolabeled spines for each category. Asterisk = significant differences  $P < 0.05$  ANOVA. Scale bar = 500 nm.

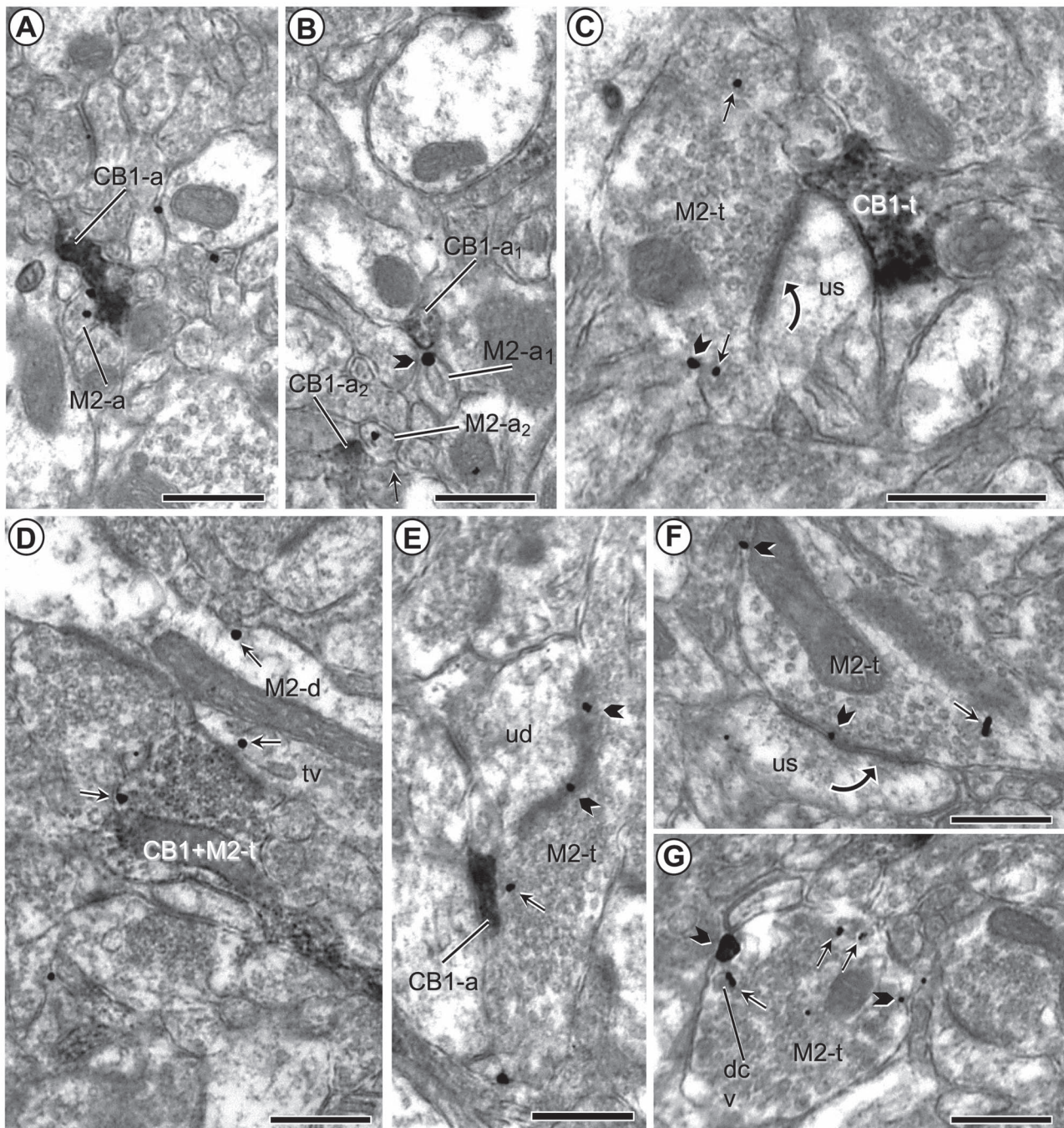


**Fig. 5.** M2R-immunogold and CB1 immunoperoxidase labeling in small axons and axon terminals. a and b) Plasmalemmal and cytoplasmic M2R immunogold is localized to small unmyelinated axons (M2-a) that are apposed to similar sized small axons that show immunoperoxidase labeling for the CB1 receptor (CB1-a). c and d) Images respectively illustrate M2R immunogold in separate axon terminals convergent on an unlabeled dendritic spine (us) and co-expressed in a single terminal presynaptic to a dendrite that also contains M2R-immunogold particles (M2-d). e and f) Presynaptic plasmalemmal and cytoplasmic distribution of M2R-immunogold particles in axon terminals forming asymmetric synapses with unlabeled dendritic spines. g) M2R immunogold is located on the plasma membrane and nearby large dense core vesicles (dcv) along the perimeter of an axon terminal without recognizable synaptic membrane specializations. Pictures in (b) and (g) were taken from THC-injected mice; all others were taken from vehicle-injected animals. Small straight arrows and black block arrows respectively indicate cytoplasmic and plasmalemmal M2R-immunogold particles in varying sizes of dendritic spines (M2-s). Black curved arrows—Asymmetric axospinous synapses; tv = tubulovesicle. Scale bars = 500 nm.

no membrane specialization were seen between M2R-labeled terminals and M2R-immunoreactive dendrites.

M2R-immunolabeled terminals made synaptic contact with unlabeled dendrites and spines receiving convergent input from CB1R-immunoreactive terminals (Fig. 5c) or apposing CB1R-labeled axons (Fig. 5e).

#### M2R localization to plasmalemmal membranes of small unmyelinated axons

The M2R immunogold was often seen on the plasma membrane of small unmyelinated axons ( $n=114$ ; Table 1a; Fig. 5a and b). About 57.9% of axonal M2R-immunogold particles were associated with the

plasmalemma. Many different types of CB1R-immunoreactive axonal profiles were observed in apposition to M2R-labeled unmyelinated axons. These included other similar unmyelinated axons (Fig. 5b) and CB1R-labeled axon terminals with synaptic vesicles and synaptic specializations. In addition, M2R-labeled small unmyelinated axons sometimes apposed M2R-immunolabeled or unlabeled dendrites and/or glial processes.

### M2R redistribution to plasmalemmal sites in dendrites of adult mice chronically receiving $\Delta 9$ -THC during adolescence

The distributions of M2R immunoreactivity and CB1R immunolabeling in the group of animals receiving  $\Delta 9$ -THC through adolescence were quite like the vehicle-injected mice in terms of number of labeled profiles and distribution of M2R immunolabeling in different types of profiles. No apparent differences were observed in general distribution parameters as assessed by contingency tests analyzing immunolabeling distribution in different profiles between vehicle and  $\Delta 9$ -THC groups either as a whole ( $X^2_9 = 9.154$ ,  $P < 0.4232$ ) or separate (single CB1R:  $X^2_1 = 0.051$ ,  $P < 0.8215$ ; single M2R:  $X^2_5 = 5.569$ ,  $P < 0.3504$ ; dual CB1R + M2R:  $X^2_1 = 0.447$ ,  $P < 0.5036$ ).

No statistical difference was observed in M2R-immunolabeled dendritic size of PL-PFC neurons between vehicle- and  $\Delta 9$ -THC-recipient mice as assessed by reliable stability in all dendritic size parameters analyzed (area,  $0.99 \pm 0.03 \mu\text{m}^2$  vs.  $0.93 \pm 0.02 \mu\text{m}^2$ ,  $F_{1,1557} = 2.89$ ;  $P < 0.0893$ ; perimeter,  $4.44 \pm 0.08 \mu\text{m}$  vs.  $4.35 \pm 0.07 \mu\text{m}$ ,  $F_{1,1557} = 0.68$ ;  $P < 0.41$ ; average diameter,  $0.56 \pm 0.009 \mu\text{m}$  vs.  $0.54 \pm 0.008 \mu\text{m}$ ,  $F_{1,1557} = 1.53$ ;  $P < 0.21$ ). However, consistently significant differences/changes were found in the plasmalemmal association of M2R immunogold between the groups of mice receiving vehicle and  $\Delta 9$ -THC. These differences are consistent with a subcellular redistribution of M2R receptors in adult mice that received chronic administration of  $\Delta 9$ -THC during adolescence. Compared with vehicle, mice receiving  $\Delta 9$ -THC showed a significant increase in plasmalemmal density of M2R immunolabeling selectively in the large dendrites (plasmalemmal particles/perimeter\*10:  $0.498 \pm 0.11/\mu\text{m}$  vs.  $0.814 \pm 0.10/\mu\text{m}$ ,  $F_{1,201} = 4.632$ ;  $P < 0.0380$ ) (Fig. 3b, d, and e). Moreover, this increase was due to specific redistribution of M2R immunogold in those dendritic segments receiving input from CB1R-immunolabeled terminals ( $F_{1,74} = 3.88$ ;  $P < 0.0264$ ) and not in those targeted exclusively by unlabeled axon terminals ( $F_{1,127} = 1.31$ ;  $P < 0.13$ ). In contrast, mice receiving vehicle or  $\Delta 9$ -THC showed no significant variations in cytoplasmic M2R-immunogold density (cytoplasmic particles/area:  $1.255 \pm 0.15/\mu\text{m}^2$  vs.  $1.413 \pm 0.14/\mu\text{m}^2$ ,  $F_{1,201} = 0.59$ ;  $P < 0.44$ ) (Fig. 3f).

### M2R redistribution in dendritic spines within the PFC of adult mice chronically receiving $\Delta 9$ -THC during adolescence

Significant differences were observed between vehicle and  $\Delta 9$ -THC groups in cytoplasmic M2R-immunogold

density within small dendritic spines. M2R-immunogold density decreased in the cytoplasmic domains of dendritic spines in  $\Delta 9$ -THC animals as observed relative to cross-sectional area (cytoplasmic particles/area:  $4.92 \pm 0.91/\mu\text{m}^2$  vs.  $1.73 \pm 0.82/\mu\text{m}^2$ ,  $F_{1,94} = 6.76$ ;  $P < 0.011$ ) (Fig. 4h). This decrease was not associated with statistically significant modifications in plasmalemmal M2R-immunolabeling density in the same group of small spines (plasmalemmal particles/perimeter\*10:  $6.61 \pm 0.68/\mu\text{m}$  vs.  $7.64 \pm 0.62/\mu\text{m}$ ,  $F_{1,94} = 1.24$ ;  $P < 0.27$ ) (Fig. 4g). The decrease in M2R cytoplasmic density in small spines was not due to changes in spine size. Mice that received vehicle or  $\Delta 9$ -THC showed no significant differences in area ( $0.085 \pm 0.004 \mu\text{m}^2$  vs.  $0.082 \pm 0.004 \mu\text{m}^2$ ,  $F_{1,94} = 0.246$ ;  $P < 0.62$ ; perimeter,  $1.30 \pm 0.038 \mu\text{m}$  vs.  $1.29 \pm 0.034 \mu\text{m}$ ,  $F_{1,94} = 0.11$ ;  $P < 0.74$ ; or average diameter,  $0.177 \pm 0.0075 \mu\text{m}$  vs.  $0.178 \pm 0.0068 \mu\text{m}$ ,  $F_{1,94} = 0.012$ ;  $P < 0.91$ ). Comparable spine sizes between animals that received either vehicle or  $\Delta 9$ -THC were also observed in the total population of spines (area,  $0.14 \pm 0.08 \mu\text{m}^2$  vs.  $0.14 \pm 0.07 \mu\text{m}^2$ ,  $F_{1,203} = 0.0014$ ;  $P < 0.97$ ; perimeter,  $1.74 \pm 0.06 \mu\text{m}$  vs.  $1.76 \pm 0.05 \mu\text{m}$ ,  $F_{1,203} = 0.11$ ;  $P < 0.73$ ; average diameter,  $0.22 \pm 0.008 \mu\text{m}$  vs.  $0.21 \pm 0.007 \mu\text{m}$ ,  $F_{1,203} = 0.043$ ;  $P < 0.84$ ).

## Discussion

Our results provide the first demonstration that chronic exposure to  $\Delta 9$ -THC during adolescence preferentially increases the plasmalemmal density of M2Rs on large dendritic profiles recipient to CB1R-containing axon terminals that form mainly inhibitory-type synapses in the PL-PFC of adults. This suggests that CB1R-mediated inhibition of the release of inhibitory neurotransmitters can modulate postsynaptic M2R responses in larger, presumably more proximal dendrites of PL-PFC neurons. We also show that M2Rs are present in medium- and small-sized dendrites and dendritic spines that more often receive asymmetric excitatory-type synapses from axon terminals lacking either M2R or CB1R. Of these dendritic profiles, only the spines show a significant treatment-specific effect of  $\Delta 9$ -THC on postsynaptic M2R expression, which is consistent with CB1R-independent postsynaptic modulation of excitatory responses in PL-PFC. These results are discussed together with their implications for understanding how cannabinoid- and non-cannabinoid-regulated M2R systems may contribute to the deleterious effects of marijuana consumption during adolescence on prefrontal cortical circuits sustaining cognitive functions in the adult (Johnston et al. 2019).

### Methodological considerations

The antisera used here have high specificity for the peptides against which they were raised as shown in previous studies (Garzón and Pickel 2006, 2016; Fitzgerald et al. 2012, 2013). Negative control experiments for all used antisera consisting in omission of the primary

antiserum from the incubation solution yielded absence of immunolabeling.

Pre-embedding immunocytochemistry achieves good ultrastructural preservation of the tissue and assures the identification of antigens that are sensitive to plastic embedding but has limited penetration of immunoreagents (Leranth and Pickel 1989). Thus, differential penetration of gold versus peroxidase in dual-labeling procedures may contribute to an underestimation of the number of labeled profiles and/or frequency of associations. Therefore, to achieve valuable quantitative analysis of dual-labeling in sections processed before plastic embedding and to minimize the probability of false negatives, we only collected ultrathin sections near the resin–tissue interface, having most complete access to immunoreagents. These precautions greatly enhanced the method reliability and partially overcame its limitations. Thus, although the quantitative values may underestimate the total number of profiles containing CB1R and M2R, they provide a good relative comparison of the cellular and subcellular distribution of the labeling patterns.

Immunogold labeling allows discrete localization of M2R to particular subcellular compartments of a given profile. Multiaggregation of particles, as well as irregular or uneven growing of silver depositions, may lead, however, to some overestimation of the plasmalemmal labeling. Both the size and morphology of the immunogold–silver particles in our tissue suggest this has been nonetheless a minor limitation in the present study.

### **CB1R distribution in axon terminals that co-express M2R or provide input to M2R-containing neurons**

The observed presence of CB1R in axon terminals forming symmetric inhibitory-type synapses confirms and extends previous descriptions of CB1R location in PL-PFC of rodents (Fitzgerald et al. 2013; Pickel et al. 2020). This distribution is like previously known descriptions in other regions such as hippocampus (Katona et al. 1999, 2006), basolateral amygdala (Katona et al. 2001), or dorsal PFC (Eggan and Lewis 2007). The activation of CB1R in these terminals likely inhibits the release of GABA and other inhibitory amino acid transmitters through coupling to Gi/o proteins and inhibition of voltage-dependent calcium channels, activation of potassium channels, and direct interference with the synaptic vesicle release mechanism as shown in earlier studies (Twitchell et al. 1997; Szabo and Schlicker 2005).

Our observation that a minor proportion of the CB1R-labeled axon terminals also contained M2Rs is consistent with convergent actions of cannabinoids and acetylcholine on the input from incoming afferents to single PL-PFC neurons. In terminals containing both receptors, the activation of either CB1R or M2R could elicit inhibition of neurotransmitter release through Gi/o protein-mediated mechanisms (Rouse et al. 2000; Schlicker and Kathmann 2001). Alternatively, CB1R activation may sequester the Gi/o proteins making

them unavailable to couple to the M2R (Schulte et al. 2012). Thus, the convergent inhibitory or antagonistic intracellular cross talk between CB1R and M2R in the PL-PFC may contribute significantly to interactions between the cannabinoid and cholinergic systems.

### **Dendritic distribution of M2R**

The present localization of M2Rs to dendrites in the PL-PFC confirms and extends prior studies showing a mainly dendritic M2R distribution in the cerebral cortex (Mrzljak et al. 1993; Volpicelli and Levey 2004). In proximal dendrites and somata, we often detected M2R labeling on cytoplasmic endomembranes or tubulovesicles, which is consistent with involvement in synthesis, transport, and/or clathrin-dependent internalization of the receptors from functional sites on plasma membrane (Decossas et al. 2003; Lambert et al. 2018). The cytoplasmic M2R distribution in cortical dendrites suggests the existence of an M2R pool for activation-dependent trafficking as agonist-induced internalization (Lambert et al. 2018). Prevalence of M2R immunogold in more distal dendrites is suggestive of different rates in receptor turnover, trafficking, or internalization. Nonsynaptic plasmalemmal M2R distribution may reflect, in part, a restricted access of the immunoreagents to the active zone (Nusser et al. 1995). These sites may, however, be those that are functionally active, insofar as M2R has a perisynaptic/extrasynaptic location when examined with a combination of labeling methods (Baude et al. 1993; Luján et al. 1996). Extrasynaptic muscarinic receptors show high affinity for their ligands and are known to be involved in nonsynaptic transmission in the cerebral cortex (Mrzljak et al. 1993; Sarter et al. 2009). Thus, the observed appositional contacts of M2R-labeled dendrites without bona fide synaptic junctions may be indicative of cellular interactions of functional relevance in the understanding of central cholinergic neurotransmission. These intriguing possibilities are consistent with the existing literature but require additional investigation to fully validate.

The observed dendritic localization of M2R near axon terminals that form mostly asymmetric excitatory-type synapses onto smaller M2R-labeled dendrites and dendritic spines suggests that excitatory neurotransmitters may modify postsynaptic responses to acetylcholine in PL-PFC. This is unexpected given the fact that most cholinergic terminals are apposed without recognizable synaptic specializations or form symmetric inhibitory-type synapses on cortical dendrites (Houser et al. 1985; Mrzljak et al. 1995; Smiley et al. 1997; Descarries et al. 2004). Conceivably, the observed unlabeled or M2R-labeled axon terminals with these types of contacts with M2R dendrites could be in fact acetylcholine-containing terminals. Likewise, acetylcholine may modulate the postsynaptic responses to glutamate and other excitatory amino acids (Seeger and Alzheimer 2001; Pickel et al. 2020) coming from either extrinsic sources or intrinsic

local neurons within the cerebral cortex (Somogyi et al. 1998; DeFelipe et al. 2002).

### M2R localization in spines

M2R labeling was detected along synaptic and extrasynaptic plasma membranes of dendritic spines, some of which received asymmetric-type inputs from axon terminals, which are often indicative of glutamatergic synapses. These latter data suggest that acetylcholine activation of M2Rs can modulate the postsynaptic excitatory responses of principal neurons that are heavily laden with dendritic spines (Mrzljak et al. 1993; Gigout et al. 2012).

### CB1R distribution in terminals contacting large-sized M2R dendrites

We detected M2R labeling in many of the dendritic targets of CB1R-containing axon terminals, many of which established symmetric synapses. This suggests possible sites for presynaptic cannabinoid modulation of GABA release (see above and Marsicano and Lutz 1999) onto neurons whose postsynaptic activity can be suppressed by acetylcholine (Seeger and Alzheimer 2001; Nuñez et al. 2012). Since cannabinoids potently inhibit GABA release in the frontal cortex (Trettel et al. 2004; Eggen and Lewis 2007), this latter distribution would facilitate cannabinoid disinhibition of the postsynaptic ACh-sensitive output neurons. Thus, based on the CB1R preferential localization in inhibitory-type terminals, cannabinoids may be able to produce similar actions to those mediated by M2R in PL-PFC neurons. Accordingly, since M2R activation induces Gi protein-coupled activation of inward rectifier potassium channels and inhibition of voltage-dependent calcium channels culminating in postsynaptic inhibition (Brown 2010), our results also favor a decreased depolarization-induced suppression of inhibition.

The observed preferential targeting of large-sized M2R-labeled dendrites by CB1R terminals suggests a major influence of CB1R-mediated cannabinoid actions on proximal dendrites nearer to the soma of output neurons and, thereby, producing potent global effects. However, since those output neurons directly affected by CB1R terminals express significantly less plasmalemmal and cytoplasmic M2R than the average, a particularly noteworthy role of cannabinoids over other neuromodulatory systems on M2R-mediated actions in PL-PFC cannot be inferred.

### M2R distribution in axons

Our present localization of M2R to axonal plasma membrane in PL-PFC is supportive of physiological experiments reporting that M2R activation inhibits transmitter release through a G protein-mediated decrease of calcium channel activation (Vannucchi and Pepeu 1995; Rouse et al. 2000; Zhang et al. 2002). Our frequent detection of M2R-labeled axonal profiles in appositional contacts without clearly defined synaptic specialization on neighboring neurons suggests a role of M2R in

nonsynaptic transmitter release from varicose axons like those of both cholinergic and monoaminergic neurons in the cerebral cortex and other brain regions (Pickel et al. 2002; Descarries et al. 2004; Fuxe et al. 2015). Nonetheless, we may have underestimated synaptic junctions formed by M2R terminals due to the preferential localization of M2R immunogold toward the perimeter of axon terminals distant from their dendritic contacts.

The M2R-labeled terminals more rarely formed axodendritic synapses with thickened postsynaptic membrane specializations that are typical of those containing glutamate (Kaneko and Fujiyama 2002). Glutamatergic inputs to the PL-PFC may originate mainly from projection neurons of the cerebral cortex or the thalamus (Nieuwenhuys 1994; Graziano et al. 2008), as well as from the basal forebrain (Henny and Jones 2008).

### Adolescent exposure to $\Delta$ 9-THC increases M2R plasmalemmal density in large dendrites recipient to CB1R terminals in adulthood

Larger dendrites recipient to CB1R-containing axon terminals showed a significant increase in plasmalemmal M2R immunogold in the PL-PFC of adult mice that received  $\Delta$ 9-THC during adolescence. Our results are consistent with prior studies showing a more predominant input from CB1R-containing axon terminals on somata and large dendrites in the cerebral cortex (Hájos and Freund 2002; Häring et al. 2012). Thus, the relative abundance of presynaptic CB1R terminals may largely account for the size-dependent effect of adolescent  $\Delta$ 9-THC on redistribution of M2R to plasmalemmal sites in large PL-PFC dendrites. However, since cytoplasmic M2R density did not change in those dendrites, the increase in plasmalemmal M2R is likely due to new synthesis or M2R mobilization to large dendrites from other neuronal domains. The level of cell surface expression of G protein-coupled receptors is a highly regulated process determining receptor subcellular compartmentalization (Hurt et al. 2013). More particularly, the balance between intracytoplasmic and plasmalemmal M2R is regulated by cholinergic environment and acetylcholine levels, such that cholinergic hypofunction enhances M2R plasmalemmal availability in cortical neurons in vitro and in vivo (Bernard et al. 2003).  $\Delta$ 9-THC administration reduces acetylcholine release in the PL-PFC (Gessa et al. 1998) and from cortical synaptosomes (Gifford et al. 2000). Moreover, chronic  $\Delta$ 9-THC treatment is known to reduce acetylcholine release in hippocampus (Nava et al. 2001). Thus, our observation of decreased M2R in plasma membranes of PL-PFC could well be a consequence, in part, of a hypocholinergic environment due to plasticity-induced changes during chronic CB1R stimulation by  $\Delta$ 9-THC treatment in adolescence.

### Adolescent exposure to $\Delta$ 9-THC decreases M2R cytoplasmic density in small spines in adulthood

Dendritic spines in PL-PFC did not receive afferent input from CB1R-labeled terminals, but they were, however,

modified by adolescent exposure to cannabinoids. The recognition of a significant decrease in M2R cytoplasmic density in small spines of the  $\Delta 9$ -THC-treated animals evidences long-term adjustments in dendritic arborizations of mice cortical neurons by cannabinoids (Fogaça et al. 2018; Kolb et al. 2018). CB1R activation recruits several intracellular signaling pathways involved in neuroplasticity, such as Akt and its downstream target GSK3 $\beta$  (Ozaita et al. 2007). Chronic exposure to  $\Delta 9$ -THC during the susceptible phase of adolescence in male mice is known to worsen cognitive function and spatial working memory (Garzón et al. 2021). Furthermore, systemic  $\Delta 9$ -THC administration increases acetylcholine release in rat PL-PFC (Acquas et al. 2001) and chronic high acetylcholine levels in the extracellular space produce M2R downregulation due to a restrained delivery from intracytoplasmic M2R stores (Bernard et al. 2003). A defective M2R distribution from the small-sized dendrites preferentially targeted by cholinergic terminals (Houser et al. 1985; Descarries et al. 2004) might well explain the changes observed in PL-PFC small spines in the  $\Delta 9$ -THC group.

## Conclusion

We conclude that M2Rs have a subcellular distribution consistent with both pre- and postsynaptic modulation of neurotransmission in the PL-PFC of adult male mice. In this region, we specifically show that CB1Rs are strategically positioned at presynaptic sites within mainly inhibitory-type axon terminals that have the potential for regulating cholinergic cortical actions mediated by M2Rs. M2R activation in dendrites postsynaptic to axon terminals containing CB1Rs could interfere with retrogradely signaled suppression of inhibition. Presynaptic M2R activation, in contrast, modulates neurotransmitter release mostly in terminals other than those responsive to CB1R-binding cannabinoids. The further demonstration that adolescent exposure to  $\Delta 9$ -THC produces long-term changes in M2R distribution within dendritic arborizations of PF-PLC neurons highly involved in cognitive and social performance could have important implications for pharmacological intervention in reducing the risk of adolescent onset psychiatric disorders.

## Funding

This research was supported by NIDA funding DA042943 to VMP and DA043982 to KM.  $\Delta 9$ -THC was provided by the Drug Supply Program of the National Institute on Drug Abuse (Bethesda, MD, USA). MG was recipient of a Spanish Science, Innovation and Universities Ministry grant (estancias de profesores e investigadores senior en centros extranjeros); reference: PR18/00436. *Conflict of interest statement:* The authors declare no competing interests.

## References

Acquas E, Pisanu A, Marrocu P, Goldberg SR, Di Chiara G. Delta9-tetrahydrocannabinol enhances cortical and hippocampal

- acetylcholine release in vivo: a microdialysis study. *Eur J Pharmacol.* 2001;419:155–161.
- Aso E, Andrés-Benito P, Ferrer I. Genetic deletion of CB1 cannabinoid receptors exacerbates the Alzheimer-like symptoms in a transgenic animal model. *Biochem Pharmacol.* 2018;157:210–216. <https://doi.org/10.1016/j.bcp.2018.08.007>.
- Bara A, Ferland JN, Rompala G, Szutorisz H, Hurd YL. Cannabis and synaptic reprogramming of the developing brain. *Nat Rev Neurosci.* 2021;22:423–438. <https://doi.org/10.1038/s41583-021-00465-5>.
- Baude Z, Nusser Z, Roberts JD, Mulvihill E, Jeffrey McIlhinney RA, Somogyi P. The metabotropic glutamate receptor (mGluR1 alpha) is concentrated at perisynaptic membrane of neuronal subpopulations as detected by immunogold reaction. *Neuron.* 1993;11:771–787.
- Bedse G, Romano A, Cianci S, Lavecchia AM, Lorenzo P, Elphick MR, LaFerla FM, Vendemiale G, Grillo C, Altieri F, et al. Altered expression of the CB1 cannabinoid receptor in the triple transgenic mouse model of Alzheimer's disease. *J Alzheimers Dis.* 2014;40:701–712. <https://doi.org/10.3233/JAD-131910>.
- Berghuis P, Rajnicek AM, Morozov YM, Ross RA, Mulder J, Urbán GM, Monory K, Marsicano G, Matteoli M, Canty A, et al. Hardwiring the brain: endocannabinoids shape neuronal connectivity. *Science.* 2007;316:1212–1216.
- Bernard V, Brana C, Liste I, Lockridge O, Bloch B. Dramatic depletion of cell surface m2 muscarinic receptor due to limited delivery from intracytoplasmic stores in neurons of acetylcholinesterase-deficient mice. *Mol Cell Neurosci.* 2003;23:121–133.
- Bodor AL, Katona I, Nyíri G, Mackie K, Ledent C, Hájos N, Freund TF. Endocannabinoid signaling in rat somatosensory cortex: laminar differences and involvement of specific interneuron types. *J Neurosci.* 2005;25:6845–6856.
- Bonner TI, Buckley NJ, Young AC, Brann MR. Identification of a family of muscarinic acetylcholine receptor genes. *Science.* 1987;237:527–532.
- Brown DA. Muscarinic acetylcholine receptors (mAChRs) in the nervous system: some functions and mechanisms. *J Mol Neurosci.* 2010;41:340–346. <https://doi.org/10.1007/s12031-010-9377-2>.
- Burston JJ, Wiley JL, Craig AA, Selley DE, Sim-Selley LJ. Regional enhancement of cannabinoid CB1 receptor desensitization in female adolescent rats following repeated  $\Delta 9$ -tetrahydrocannabinol exposure. *Br J Pharmacol.* 2010;161:103–112.
- Castillo PE, Younts TJ, Chávez AE, Hashimoto Y. Endocannabinoid signaling and synaptic function. *Neuron.* 2012;76:70–81. <https://doi.org/10.1016/j.neuron.2012.09.020>.
- Chan J, Aoki C, Pickel VM. Optimization of differential immunogold-silver and peroxidase labeling with maintenance of ultrastructure in brain sections before plastic embedding. *J Neurosci Methods.* 1990;33:113–127.
- Chen H-T, Mackie K. Adolescent  $\Delta^9$ -tetrahydrocannabinol exposure selectively impairs working memory but not several other mPFC-mediated Behaviors. *Front Psych.* 2020;11:576214. <https://doi.org/10.3389/fpsy.2020.576214>.
- Decossas M, Bloch B, Bernard V. Trafficking of the muscarinic m2 autoreceptor in cholinergic basalocortical neurons in vivo: differential regulation of plasma membrane receptor availability and intraneuronal localization in acetylcholinesterase-deficient and -inhibited mice. *J Comp Neurol.* 2003;462:302–314.
- DeFelipe J, Alonso-Nanclares L, Arellano JI. Microstructure of the neocortex: comparative aspects. *J Neurocytol.* 2002;31:299–316.
- Descarries L, Mechawar N, Aznavour N, Watkins KC. Structural determinants of the roles of acetylcholine in cerebral cortex. *Prog Brain Res.* 2004;145:45–58.

- Egerton A, Allison C, Brett RR, Pratt JA. Cannabinoids and prefrontal cortical function: insights from preclinical studies. *Neurosci Biobehav Rev*. 2006;30:680–695.
- Egertová M, Elphick MR. Localisation of cannabinoid receptors in the rat brain using antibodies to the intracellular C-terminal tail of CB. *J Comp Neurol*. 2000;422:159–171.
- Eggen SM, Lewis DA. Immunocytochemical distribution of the cannabinoid CB1 receptor in the primate neocortex: a regional and laminar analysis. *Cereb Cortex*. 2007;17:175–191.
- Fitzgerald ML, Chan J, Mackie K, Lupica CR, Pickel VM. Altered dendritic distribution of dopamine D2 receptors and reduction in mitochondrial number in parvalbumin-containing interneurons in the medial prefrontal cortex of cannabinoid-1 (CB1) receptor knockout mice. *J Comp Neurol*. 2012;520:4013–4031. <https://doi.org/10.1002/cne.23141>.
- Fitzgerald ML, Mackie K, Pickel VM. The impact of adolescent social isolation on dopamine D2 and cannabinoid CB1 receptors in the adult rat prefrontal cortex. *Neuroscience*. 2013;235:40–50. <https://doi.org/10.1016/j.neuroscience.2013.01.021>.
- Fogaça MV, Campos AC, Coelho LD, Duman RS, Guimarães FS. The anxiolytic effects of cannabidiol in chronically stressed mice are mediated by the endocannabinoid system: role of neurogenesis and dendritic remodeling. *Neuropharmacology*. 2018;135:22–33. <https://doi.org/10.1016/j.neuropharm.2018.03.001>.
- Fuxe K, Agnati LF, Marcoli M, Borroto-Escuela DO. Volume transmission in central dopamine and noradrenaline neurons and its Astroglial targets. *Neurochem Res*. 2015;40:2600–2614. <https://doi.org/10.1007/s11064-015-1574-5>.
- Garzón M, Pickel VM. Dendritic and axonal targeting of the vesicular acetylcholine transporter to membranous cytoplasmic organelles in laterodorsal and pedunculopontine tegmental nuclei. *J Comp Neurol*. 2000;419:32–48.
- Garzón M, Pickel VM. Subcellular distribution of M2 muscarinic receptors in relation to dopaminergic neurons of the rat ventral tegmental area. *J Comp Neurol*. 2006;498:821–839.
- Garzón M, Pickel VM. Electron microscopic localization of M2-muscarinic receptors in cholinergic and noncholinergic neurons of the laterodorsal tegmental and pedunculopontine nuclei of the rat mesopontine tegmentum. *J Comp Neurol*. 2016;524:3084–3103. <https://doi.org/10.1002/cne.24010>.
- Garzón M, Vaughan RA, Uhl GR, Kuhar MJ, Pickel VM. Cholinergic axon terminals in the ventral tegmental area target a subpopulation of neurons expressing low levels of the dopamine transporter. *J Comp Neurol*. 1999;410:197–210.
- Garzón M, Wang G, Chan J, Bourie F, Mackie K, Pickel VM. Adolescent administration of  $\Delta^9$ -THC decreases the expression and function of muscarinic-1 receptors in prelimbic prefrontal cortical neurons of adult male mice. *IBRO Neurosci Rep*. 2021;11:144–155.
- Gessa GL, Casu MA, Carta G, Mascia MS. Cannabinoids decrease acetylcholine release in the medial-prefrontal cortex and hippocampus, reversal by SR 141716A. *Eur J Pharmacol*. 1998;355:119–124.
- Gifford AN, Bruneus M, Gatley SJ, Volkow ND. Cannabinoid receptor-mediated inhibition of acetylcholine release from hippocampal and cortical synaptosomes. *Br J Pharmacol*. 2000;131:645–650.
- Gigout S, Jones GA, Wierschke S, Davies CH, Watson JM, Deisz RA. Distinct muscarinic acetylcholine receptor subtypes mediate pre- and postsynaptic effects in rat neocortex. *BMC Neurosci*. 2012;13:42. <https://doi.org/10.1186/1471-2202-13-42>.
- Gray EG. Axo-somatic and axo-dendritic synapses of the cerebral cortex: an electron microscope study. *J Anat*. 1959;93:420–433.
- Graziano A, Liu XB, Murray KD, Jones EG. Vesicular glutamate transporters define two sets of glutamatergic afferents to the somatosensory thalamus and two thalamocortical projections in the mouse. *J Comp Neurol*. 2008;507:1258–1276. <https://doi.org/10.1002/cne.21592>.
- Gruber AJ, Pope HG Jr. Marijuana use among adolescents. *Pediatr Clin N Am*. 2002;49:389–413.
- Hájos N, Freund TF. Distinct cannabinoid sensitive receptors regulate hippocampal excitation and inhibition. *Chem Phys Lipids*. 2002;121:73–82.
- Hájos N, Papp EC, Acsády L, Levey AI, Freund TF. Distinct interneuron types express m2 muscarinic receptor immunoreactivity on their dendrites or axon terminals in the hippocampus. *Neuroscience*. 1998;82:355–376.
- Häring M, Guggenhuber S, Lutz B. Neuronal populations mediating the effects of endocannabinoids on stress and emotionality. *Neuroscience*. 2012;204:145–158.
- Heidbreder CA, Groenewegen HJ. The medial prefrontal cortex in the rat: evidence for a dorso-ventral distinction based upon functional and anatomical characteristics. *Neurosci Biobehav Rev*. 2003;27:555–579.
- Henny P, Jones BE. Projections from basal forebrain to prefrontal cortex comprise cholinergic, GABAergic and glutamatergic inputs to pyramidal cells or interneurons. *Eur J Neurosci*. 2008;27:654–670. <https://doi.org/10.1111/j.1460-9568.2008.06029.x>.
- Herkenham M, Lynn AB, De Costa BR, Richfield EK. Neuronal localization of cannabinoid receptors in the basal ganglia of the rat. *Brain Res*. 1991;547:267–274.
- Herkenham M, Lynn AB, Johnson MR, Melvin LS, De Costa BR, Rice KC. Characterization and localization of cannabinoid receptors in rat brain: a quantitative in vitro autoradiographic study. *J Neurosci*. 1991;11:563–583.
- Hohmann CF, Potter ED, Levey AI. Development of muscarinic receptor subtypes in the forebrain of the mouse. *J Comp Neurol*. 1995;358:88–101.
- Houser CR, Crawford GD, Salvaterra PM, Vaughn JE. Immunocytochemical localization of choline acetyltransferase in rat cerebral cortex: a study of cholinergic neurons and synapses. *J Comp Neurol*. 1985;234:17–34.
- Hsu SM, Raine L, Fanger H. Use of avidin-biotin-peroxidase complex (ABC) in immunoperoxidase techniques: a comparison between ABC and unlabeled antibody (PAP) procedures. *J Histochem Cytochem*. 1981;29:577–580.
- Hurt CM, Ho VK, Angelotti T. Systematic and quantitative analysis of G protein-coupled receptor trafficking motifs. *Methods Enzymol*. 2013;521:171–187. <https://doi.org/10.1016/B978-0-12-391862-8.00009-0>.
- Johnston LD, Miech RA, O'Malley PM, Bachman JG, Schulenberg JE, Patrick ME. *Monitoring the future national survey results on drug use 1975–2018: overview, key findings on adolescent drug use*. Ann Arbor: Institute for Social Research, University of Michigan; 2019.
- Kaneko T, Fujiyama F. Complementary distribution of vesicular glutamate transporters in the central nervous system. *Neurosci Res*. 2002;42:243–250.
- Kathmann M, Weber B, Schlicker E. Cannabinoid CB1 receptor-mediated inhibition of acetylcholine release in the brain of NMRI, CD-1 and C57BL/6J mice. *Naunyn Schmiedeberg's Arch Pharmacol*. 2001;363:50–56.
- Katona I, Urbán GM, Wallace M, Ledent C, Jung KM, Piomelli D, Mackie K, Freund TF. Molecular composition of the endocannabinoid system at glutamatergic synapses. *J Neurosci*. 2006;26:5628–5637.
- Katona I, Sperlágħ B, Sik A, Káfalvi A, Vizi ES, Mackie K, Freund TF. Presynaptically located CB1 cannabinoid receptors regulate

- GABA release from axon terminals of specific hippocampal interneurons. *J Neurosci*. 1999;19:4544–4558.
- Katona I, Rancz EA, Acsady L, Ledent C, Mackie K, Hájos N, Freund TF. Distribution of CB1 cannabinoid receptors in the amygdala and their role in the control of GABAergic transmission. *J Neurosci*. 2001;21:9506–9518.
- Kishimoto Y, Kano M. Endogenous cannabinoid signaling through the CB1 receptor is essential for cerebellum-dependent discrete motor learning. *J Neurosci*. 2006;26:8829–8837.
- Kolb B, Li Y, Robinson T, Parker LA. THC alters morphology of neurons in medial prefrontal cortex, orbital prefrontal cortex, and nucleus accumbens and alters the ability of later experience to promote structural plasticity. *Synapse*. 2018;72(3):e22020. <https://doi.org/10.1002/syn.22020>.
- Laaris N, Good CH, Lupica CR. Delta9-tetrahydrocannabinol is a full agonist at CB1 receptors on GABA neuron axon terminals in the hippocampus. *Neuropharmacology*. 2010;59:121–127.
- Lambert L, Dubayle D, Fafouri A, Herzog E, Csaba Z, Dournaud P, El Mestikawy S, Bernard V. Endocytosis of activated muscarinic m2 receptor (m2R) in live mouse hippocampal neurons occurs via a Clathrin-dependent pathway. *Front Cell Neurosci*. 2018;12:450. <https://doi.org/10.3389/fncel.2018.00450.eCollection2018>.
- Leranth C, Pickel VM. Electron microscopic preembedding double immunostaining methods. In: Heimer L, Zaborsky L, editors. *Tract tracing methods 2, recent progress*. New York: Plenum; 1989. pp. 129–172
- Levey AI, Kitt CA, Simonds WF, Price DL, Brann MR. Identification and localization of muscarinic acetylcholine receptor proteins in brain with subtype-specific antibodies. *J Neurosci*. 1991;11:3218–3226.
- Lopez-Rodriguez AB, Llorente-Berzal A, Garcia-Segura LM, Viveros M-P. Sex-dependent long-term effects of adolescent exposure to THC and/or MDMA on neuroinflammation and serotonergic and cannabinoid systems in rats. *Br J Pharmacol*. 2014;171:1435–1447.
- Luján R, Nusser Z, Roberts JD, Shigemoto R, Somogyi P. Perisynaptic location of metabotropic glutamate receptors mGluR1 and mGluR5 on dendrites and dendritic spines in the rat hippocampus. *Eur J Neurosci*. 1996;8:1488–1500.
- Marsicano G, Lutz B. Expression of the cannabinoid receptor CB1 in distinct neuronal subpopulations in the adult mouse forebrain. *Eur J Neurosci*. 1999;11:4213–4225.
- Matsuda LA, Bonner TI, Lolait SJ. Localization of cannabinoid receptor mRNA in rat brain. *J Comp Neurol*. 1993;327:535–550.
- Milner TA, Waters EM, Robinson DC, Pierce JP. Degenerating processes identified by electron microscopic immunocytochemical methods. *Methods Mol Biol*. 2011;793:23–59. [https://doi.org/10.1007/978-1-61779-328-8\\_3](https://doi.org/10.1007/978-1-61779-328-8_3).
- Mishima K, Egashira N, Matsumoto Y, Iwasaki K, Fujiwara M. Involvement of reduced acetylcholine release in Delta9-tetrahydrocannabinol-induced impairment of spatial memory in the 8-arm radial maze. *Life Sci*. 2002;72:397–407.
- Mrzljak L, Levey AI, Goldman-Rakic PS. Association of m1 and m2 muscarinic receptor proteins with asymmetric synapses in the primate cerebral cortex: morphological evidence for cholinergic modulation of excitatory neurotransmission. *Proc Natl Acad Sci U S A*. 1993;90:5194–5198.
- Mrzljak L, Pappy M, Leranth C, Goldman-Rakic PS. Cholinergic synaptic circuitry in the macaque prefrontal cortex. *J Comp Neurol*. 1995;357:603–617.
- Mrzljak L, Levey AI, Belcher S, Goldman-Rakic PS. Localization of the m2 muscarinic acetylcholine receptor protein and mRNA in cortical neurons of the normal and cholinergically deafferented rhesus monkey. *J Comp Neurol*. 1998;390:112–132.
- Nava F, Carta G, Colombo G, Gessa GL. Effects of chronic Delta(9)-tetrahydrocannabinol treatment on hippocampal extracellular acetylcholine concentration and alternation performance in the T-maze. *Neuropharmacology*. 2001;41:392–399.
- Nieuwenhuys R. The neocortex. An overview of its evolutionary development, structural organization and synaptology. *Anat Embryol*. 1994;190:307–337.
- Nuñez A, Domínguez S, Buño W, Fernández de Sevilla D. Cholinergic-mediated response enhancement in barrel cortex layer V pyramidal neurons. *J Neurophysiol*. 2012;108:1656–1668. <https://doi.org/10.1152/jn.00156.2012>.
- Nusser Z, Roberts JD, Baude A, Richards JG, Somogyi P. Relative densities of synaptic and extrasynaptic GABA receptors on cerebellar granule cells as determined by a quantitative immunogold method. *J Neurosci*. 1995;15:2948–2960.
- Ong WY, Mackie K. A light and electron microscopic study of the CB1 cannabinoid receptor in primate brain. *Neuroscience*. 1999;92:1177–1191.
- Ozaita A, Puighermanal E, Maldonado R. Regulation of PI3K/Akt/GSK-3 pathway by cannabinoids in the brain. *J Neurochem*. 2007;102:1105–1114.
- Paxinos G, Franklin KBJ. *The mouse brain in stereotaxic coordinates*. San Diego: Academic Press; 2001
- Peralta EG, Winslow JW, Peterson GL, Smith DH, Ashkenazi A, Ramachandran J, Schimerlik MI, Capon DJ. Primary structure and biochemical properties of an M2 muscarinic receptor. *Science*. 1987;236:600–605.
- Peters A, Palay SL, Webster H. *The fine structure of the nervous system*. New York: Oxford University Press; 1991
- Pickel VM, Garzón M, Mengual E. Electron microscopic immunolabeling of transporters and receptors identifies transmitter-specific functional sites envisioned in Cajal's neuron. *Prog Brain Res*. 2002;136:145–155.
- Pickel VM, Bourie F, Chan J, Mackie K, Lane DA, Wang G. Chronic adolescent exposure to Δ9-tetrahydrocannabinol decreases NMDA current and extrasynaptic plasmalemmal density of NMDA GluN1 subunits in the prefrontal cortex of adult male mice. *Neuropsychopharmacology*. 2020;45:374–383. <https://doi.org/10.1038/s41386-019-0466-9> [Epub ahead of print].
- Reynolds ES. The use of lead citrate at high pH as an electron-opaque stain in electron microscopy. *J Cell Biol*. 1963;17:208–212.
- Rouse ST, Edmunds SM, Yi H, Gilmore ML, Levey AI. Localization of M(2) muscarinic acetylcholine receptor protein in cholinergic and non-cholinergic terminals in rat hippocampus. *Neurosci Lett*. 2000;284:182–186.
- Rubino T, Parolaro D. Long lasting consequences of cannabis exposure in adolescence. *Mol Cell Endocrinol*. 2008;286:S108–S113. <https://doi.org/10.1016/j.mce.2008.02.003>.
- Rubino T, Parolaro D. The impact of exposure to cannabinoids in adolescence: insights from animal models. *Biol Psychiatry*. 2016;79:578–585. <https://doi.org/10.1016/j.biopsych.2015.07.024>.
- Rubino T, Prini P, Piscitelli F, Zamberletti E, Trusel M, Melis M, Sgheddu C, Ligresti A, Tonini R, di Marzo V, et al. Adolescent exposure to THC in female rats disrupts developmental changes in the prefrontal cortex. *Neurobiol Dis*. 2015;73:60–69. <https://doi.org/10.1016/j.nbd.2014.09.015>.

- Sarter M, Parikh V, Howe WM. Phasic acetylcholine release and the volume transmission hypothesis: time to move on. *Nat Rev Neurosci*. 2009;10:383–390. <https://doi.org/10.1038/nrn2635>.
- Schlicker E, Kathmann M. Modulation of transmitter release via presynaptic cannabinoid receptors. *Trends Pharmacol Sci*. 2001;22:565–572.
- Schulte K, Steingrüber N, Jergas B, Redmer A, Kurz CM, Buchalla R, Lutz B, Zimmer A, Schlicker E. Cannabinoid CB1 receptor activation, pharmacological blockade, or genetic ablation affects the function of the muscarinic auto- and heteroreceptor. *Naunyn Schmiedeberg's Arch Pharmacol*. 2012;385:385–396. <https://doi.org/10.1007/s00210-011-0717-8>.
- Seeger T, Alzheimer C. Muscarinic activation of inwardly rectifying K(+) conductance reduces EPSPs in rat hippocampal CA1 pyramidal cells. *J Physiol*. 2001;535:383–396.
- Smiley JF, Morrell F, Mesulam MM. Cholinergic synapses in human cerebral cortex: an ultrastructural study in serial sections. *Exp Neurol*. 1997;144:361–368.
- Somogyi P, Tamás G, Lujan R, Buhl EH. Salient features of synaptic organisation in the cerebral cortex. *Brain Res Brain Res Rev*. 1998;26:113–135.
- Spear LP. The adolescent brain and age-related behavioral manifestations. *Neurosci Biobehav Rev*. 2000;24:417–463.
- Steiner H, Bonner TI, Zimmer AM, Kitai ST, Zimmer A. Altered gene expression in striatal projection neurons in CB1 cannabinoid receptor knockout mice. *Proc Natl Acad Sci U S A*. 1999;96:5786–5790.
- Szabo B, Schlicker E. Effects of cannabinoids on neurotransmission. *Handb Exp Pharmacol*. 2005;168:327–365.
- Trettel J, Fortin DA, Levine ES. Endocannabinoid signalling selectively targets perisomatic inhibitory inputs to pyramidal neurones in juvenile mouse neocortex. *J Physiol*. 2004;556:95–107.
- Twitchell W, Brown S, Mackie K. Cannabinoids inhibit N- and P/Q-type calcium channels in cultured rat hippocampal neurons. *J Neurophysiol*. 1997;78:43–50. <https://doi.org/10.1152/jn.1997.78.1.43>.
- Vannucchi MG, Pepeu G. Muscarinic receptor modulation of acetylcholine release from rat cerebral cortex and hippocampus. *Neurosci Lett*. 1995;190:53–56.
- Vilaró MT, Wiederhold KH, Palacios JM, Mengod G. Muscarinic M2 receptor mRNA expression and receptor binding in cholinergic and non-cholinergic cells in the rat brain: a correlative study using in situ hybridization histochemistry and receptor autoradiography. *Neuroscience*. 1992;47:367–393.
- Vilaró MT, Palacios JM, Mengod G. Multiplicity of muscarinic autoreceptor subtypes? Comparison of the distribution of cholinergic cells and cells containing mRNA for five subtypes of muscarinic receptors in the rat brain. *Mol Brain Res*. 1994;21:30–46.
- Volpicelli LA, Levey AI. Muscarinic acetylcholine receptor subtypes in cerebral cortex and hippocampus. *Prog Brain Res*. 2004;145:59–66.
- Wager-Miller J, Westbroek R, Mackie K. Dimerization of G protein-coupled receptors: CB1 cannabinoid receptors as an example. *Chem Phys Lipids*. 2002;121:83–89.
- Wang L, Yuan LL. Activation of M2 muscarinic receptors leads to sustained suppression of hippocampal transmission in the medial prefrontal cortex. *J Physiol*. 2009;587:5139–5147. <https://doi.org/10.1113/jphysiol.2009.174821>.
- Weiner DM, Levey AI, Brann MR. Expression of muscarinic acetylcholine and dopamine receptor mRNAs in rat basal ganglia. *Proc Natl Acad Sci U S A*. 1990;87:7050–7054.
- Wise LE, Varvel SA, Selley DE, Wiebelhaus JM, Long KA, Middleton LS, Sim-Selley LJ, Lichtman AH, et al. Delta(9)-tetrahydrocannabinol-dependent mice undergoing withdrawal display impaired spatial memory. *Psychopharmacology*. 2011;217:485–494.
- Zhang W, Basile AS, Gomeza J, Volpicelli LA, Levey AI, Wess J. Characterization of central inhibitory muscarinic autoreceptors by the use of muscarinic acetylcholine receptor knock-out mice. *J Neurosci*. 2002;22:1709–1717.